VYSOKÉ UČENÍ TECHNICKÉ V BRNĚ

BRNO UNIVERSITY OF TECHNOLOGY

FAKULTA STROJNÍHO INŽENÝRSTVÍ
ÚSTAV FYZIKÁLNÍHO INŽENÝRSTVÍ

FACULTY OF MECHANICAL ENGINEERING
INSTITUTE OF PHYSICAL ENGINEERING

PREPARATION AND APPLICATION OF METAL AND SEMICONDUCTOR NANOSTRUCTURES

PŘÍPRAVA A APLIKACE KOVOVÝCH A POLOVODIČOVÝCH NANOSTRUKTUR

BAKALÁŘSKÁ PRÁCE
BACHELOR'S THESIS

AUTOR PRÁCE — JAKUB HRUBÝ
AUTHOR

VEDOUCÍ PRÁCE — RNDr. MICHAELA ŠIMŠÍKOVÁ, Ph.D.
SUPERVISOR

BRNO 2015

Vysoké učení technické v Brně, Fakulta strojního inženýrství

Ústav fyzikálního inženýrství
Akademický rok: 2014/2015

ZADÁNÍ BAKALÁŘSKÉ PRÁCE

student(ka): Jakub Hrubý

který/která studuje v **bakalářském studijním programu**

obor: **Fyzikální inženýrství a nanotechnologie (3901R043)**

Ředitel ústavu Vám v souladu se zákonem č.111/1998 o vysokých školách a se Studijním a zkušebním řádem VUT v Brně určuje následující téma bakalářské práce:

Příprava a aplikace kovových a polovodičových nanostruktur

v anglickém jazyce:

Preparation and application of metal and semiconductor nanostructures

Stručná charakteristika problematiky úkolu:

Nanočástice jsou jedinečné pro své fyzikálně-chemické vlastnosti, díky kterým mají široké možnosti využití v mnoha odvětvích průmyslu a medicíny.

Cíle bakalářské práce:

- Zpracování literárního přehledu o přípravě nanočástic,
- příprava nanostruktur různých velikosti a morfologii,
- charakterizace připravených struktur,
- aplikace připravených nanostruktur.

Seznam odborné literatury:

[1] D. L. Fedlheim, C.A. Foss, Metal Nanoparticles: Synthesis, Characterization, and Applications, CRC Press, Boca Raton, 2002.
[2] B. I. Kharisov, O.V. Kharissova, U. Ortiz-Mendez, Handbook of Less-Common Nanostructures, CRC Press, Boca Raton, 2012.
[3] R. Nagarajan, T. Alan Hatton: Nanoparticles: Synthesis, Stabilization, Passivation, and Functionalization, Oxford University Press, USA, 2008.

Vedoucí bakalářské práce: RNDr. Michaela Šimšíková, Ph.D.

Termín odevzdání bakalářské práce je stanoven časovým plánem akademického roku 2014/2015.

V Brně, dne 13.10.2014

L.S.

prof. RNDr. Tomáš Šikola, CSc. Ředitel ústavu	doc. Ing. Jaroslav Katolický, Ph.D. Děkan fakulty

ABSTRACT

This bachelor's thesis deals with theoretical background concerning basics of preparation, characterization, and possible applications of nanostructures. Experimental part provides guidance through synthesis and characterization of nanostructures. Noble metal nanoparticles are represented by gold and silver. In addition, zinc oxide II-VI semiconductor and copper oxide – zinc oxide composite were synthesized by the bottom up method as well. Various shapes of particles were achieved such as spheres, rods, cobblestones, and so called nanoflowers. Prepared nanoparticles were then characterized. Optical microscopy was performed for approximate estimation of morphology. Scanning electron microscopy was used for detailed insight into a structure of samples. Other characterization methods involve photoluminiscence and absorbance which were applied in CuO/ZnO composite characterization.

KEYWORDS

bottom-up preparation method, nucleation and growth, hydrothermal synthesis, colloidal solutions, metallic nanoparticles, metal oxide nanoparticles, characterization, possible applications

ABSTRAKT

Tato práce se zabývá teoretickými základy přípravy, charakterizace a možnými aplikací nanostruktur. V experimentální části je nastíněna syntéza a charakterizace nanostruktur. Ušlechtilé kovy jsou zastoupeny zlatem a stříbrem. Oxid zinečnatý jakožto II–VI polovodič a kompozit oxidu zinečnatého a oxidu měďnatého byly také syntetizovány bottom-up metodou. Připravené částice tvořily různé tvary, jako například kuličky, tyčinky, dlaždičky a takzvané nanokytičky. Částice byly posléze charakterizovány. Optickou mikroskopií byl proveden přibližný odhad morfologie. Skenovací elektronový mikroskop byl použit pro detailní pohled do struktury vzorku. Další charakterizační metody jako fotoluminiscence a absorbance byly využity u CuO/ZnO kompozitu.

KLÍČOVÁ SLOVA

příprava metodou bottom-up, nukleace a růst, hydrotermální syntéza, koloidní roztoky, kovové nanočástice, nanočástice oxidů kovů, charakterizace, možné aplikace

HRUBÝ, Jakub *Preparation and application of metal and semiconductor nanostructures*: bachelor's thesis. Brno: Brno University of Technology, Faculty of Mechanical Engineering, Institute of Physical Engineering, 2015. 44 p. Supervised by RNDr. Michaela Šimšíková, Ph.D.

DECLARATION

I declare that I have elaborated my bachelor's thesis on the theme of "Preparation and application of metal and semiconductor nanostructures" independently, under the supervision of the bachelor's thesis supervisor and with the use of technical literature and other sources of information which are all quoted in the thesis and detailed in the list of literature at the end of the thesis.

As the author of the bachelor's thesis I furthermore declare that, concerning the creation of this bachelor's thesis, I have not infringed any copyright. In particular, I have not unlawfully encroached on anyone's personal copyright and I am fully aware of the consequences in the case of breaking Regulation § 11 and the following of the Copyright Act No 121/2000 Vol., including the possible consequences of criminal law resulted from Regulation § 152 of Criminal Act No 140/1961 Vol.

Brno ....

(author's signature)

Acknowledgement

Rád bych poděkoval vedoucí práce RNDr. Michaele Šimšíkové Ph.D. za odborné vedení, užitečné rady a cenné připomínky. Dále bych chtěl poděkovat celému kolektivu Ústavu fyzikálního inženýrství za výborné prostředí umožňující vznik práce.
Speciální poděkování patří přítelkyni a rodině za poskytnutí duševní a materiální podpory.

Analýzy vzorků byly provedeny ve Sdílené laboratoři přípravy a charakterizace nanostruktur CEITEC VUT a hrazeny z projektu CEITEC - open access LM2011020.

Jakub Hrubý

CONTENTS

1 INTRODUCTION

Nanotechnology is quite new and progressive branch of natural sciences nowadays. It deals with structures in the nanometre scale (i.e. $1\,\mathrm{nm} = 10^{-9}\,\mathrm{m}$). The nano–technology also involves manufacturing, controlling, and manipulating of matter. A nanoparticle is a building block in fabrication of a nanostructure. These objects are smaller than common macroscopic objects described by Newton's motion laws, but mostly bigger than an atomic structure which exhibits phenomenons of quantum mechanics. According to different organizations [1], there are several definitions of the nanoparticle. Nanoparticles could be defined as particles with size in the range of 1 to 100 nm in at least one of three dimensions. Apparently, size does matter, due to their smallness, they possess unique inherent properties. This includes high ratio of atoms/molecules spread on the particle surface rather than in the interior and immense surface area available per unit volume of the material. Extent of both of these characteristics increase with a decreasing nanoparticle size. Moreover, unique physical, chemical, and biological properties arise from these features [2].

There are two fundamentally different approaches of preparation of nanoparticles. The first one is a breakdown method (top–down) and has been known since ancient times. This method is based on application of external force in order to break down material into smaller pieces. Rising surface energy leads to more probable aggregation of particles. Therefore, particles refined by this approach are usually limited to size of the final particle at the extent of a few micrometres. Characteristic techniques of top–down approach are grinding, milling, and mechanical alloying. The second approach is addressed as a build up (bottom–up) method. Gaseous phase methods and liquid phase methods belong to this category. The most common gaseous phase methods are the chemical vapour deposition (CVD) which involves a chemical reaction, and the physical vapour deposition (PVD) which uses cooling of the evaporated material. Nevertheless, liquid phase methods play the prime role in the preparation of nanoparticles. Further division contains liquid/liquid and sedimentation method. Typical example of the first preparation method is chemical reduction of metal ions. The oxidation state of zero is obtained for metal (i.e. $\mathrm{M}^{n+} \rightarrow \mathrm{M}^{0}$). The biggest advantages of this method are facile fabrication of variously shaped nanoparticles, high yields, and reasonable expenses. The latter refers to a sol–gel process, that is mainly used for fabrication of metal oxide nanoparticles. Bottom up approach gives freedom in preparation of a final product. On the contrary, impurities and particles stability are matter of concern. Preparation procedure should be selected according to nanoparticles size and distribution demand [1].

Nanoparticles by itself offer a large variety of possible applications. The very first signs of the use of the particles in the nanoscale date back to first few centuries AD. The ancient Rome glass industry masterpiece, the Lycurgus cup, is perhaps one of the most famous preserved relics. Nowadays, the cup is at the exhibition of the British Museum. The speciality of this cup lies in a dichroic glass which was used in the cup. Modern dichroic glass is used for example in a dichroic filter. Research of these filters is carried out by NASA and its associates [3]. When the cup is lit from the front, a viewer observes the green opaque cup. On the contrary, when the light source is behind or inside the cup, the viewer observes translucent red cup. The inner structure of the cup was unveiled by modern characteristic technique, transmission electron microscopy. Tiny particles of 50–100 nm in size from gold:silver alloy, in ratio of 3:7, were found [4]. During the Middle Ages, early nanotechnology was present in the form of stained glass inside churches. New impulse to nanotechnology *per se* was during the 20th century. Along with rapid burst of technology, new characterization methods such as electron microscopy and atomic force microscopy emerged. Famous R. Feynman's lecture "There's Plenty of Room at the Bottom" was given at meeting at Caltech on December 29, 1959 [5]. The lecture significantly motivated and still motivates scientists all over the world in the field of nanotechnology. Possible applications are the driving force of present research. Biomedicine, consumer goods, personal care products, electronics, computers, engineering materials, treatment of environment, food–processing industry, energetics, transportation, and many more segments can be enhanced with the nanotechnology [2].

2 THEORETICAL BACKGROUND

Basic characteristics of the nanostructure and fundamental theory related to the preparation, characterization, and application is provided in this chapter. The small particle size is a carrier of extraordinary features. For instance, absorbance and emission wavelengths can be controlled by the size or surface functionalization of the particle. Transparency for visible light wavelengths can be achieved by exploiting and overcoming the critical wavelength of light. Hence, ionic potential and electron affinity which correspond to the electron transport properties are also utilizable. These features are also size dependant. For metals, with the decrease of size, the sintering and melting temperatures decrease. Nanoparticles incorporated in a solid matter matrix can provide better thermal conductivity. Individual metallic magnetic nanoparticles can exhibit superparamagnetic behaviour. In addition, catalysis can be enhanced by huge surface area per unit volume feature. Recent research emphasis is put on control over size and utilization of the characteristic interface properties [2].

2.1 Distinctive properties of nanostructures

Unique properties of nanostructures emerge markedly from the nanoscopic scale. One can not simply extrapolate properties from a bulk material to a nanoparticle. Ability to adapt the theoretical assumptions according to the scale is important. An intermediate particle between an atomic scope and the bulk material is referred to as a quantum dot (QD). Quantum dots are usually units of nanometres long.

For instance, in an atom, negatively charged electrons orbit around a positively charged nucleus. Number of electrons depends solely on the element. In the simplest case, the hydrogen atom, just one electron orbits around one proton. Calculations of the hydrogen atom can be solved analytically. As soon as more than one electron is involved, additional aspects to a standard electron–nucleus interaction such as electron–electron interaction have to be taken into account. The energy states of multi–electron atoms are more likely calculated by the Hartree–Fock approximation method. In this method, each electron is ascribed to an individual orbit addressed as the atomic orbital (AO) with the associated discrete energy level. Depending on the angular momentum of the orbit, atomic orbitals have spherical (s–orbital), club–like (p–orbital), or rather complicated (d–, f–orbitals) shape. Shared orbitals between the atoms, molecular orbitals (MOs), are formed from the combination of bonding (σ) and anti–bonding (σ^*) orbital. Molecular orbitals occupation principles are driven by the Pauli's exclusion principle and Hund's rules [6].

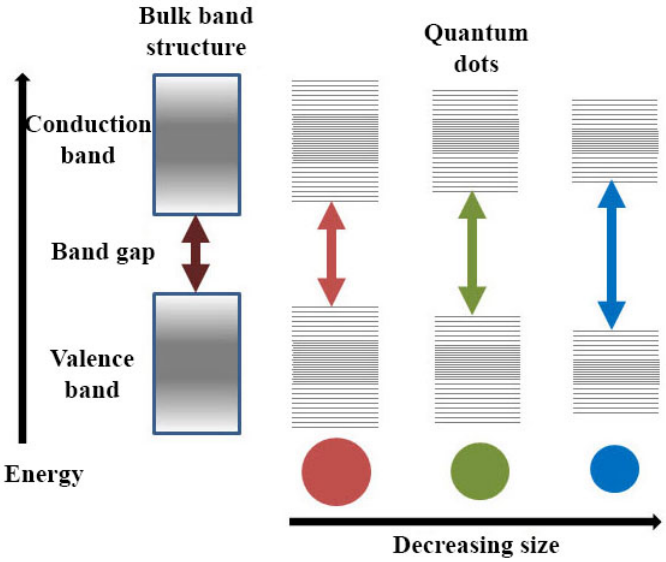

Fig. 2.1: Splitting of energy levels in quantum dots due to the quantum confinement effect. The band gap broadens with decrease in size of the nanocrystal. Edges of the conduction and valence band often exhibit discrete energy levels, whereas bigger quantum dots incline to the continual bulk material behaviour. From ref. [7], [8].

Huge surface over volume ratio is a good example of another virtue of the nanostructures. For example, Au nanoparticles with 4.9 nm in diameter are constituted by 15 % of atoms exposed on the surface. However, almost twice smaller Au nanoparticles with 2.7 nm in diameter have 52 % of atoms exposed on the surface. This immense surface area of small nanostructures comes hand in hand with increased reactivity. Therefore, nanoparticles are a good promise for the next generation of catalysts [1], [9].

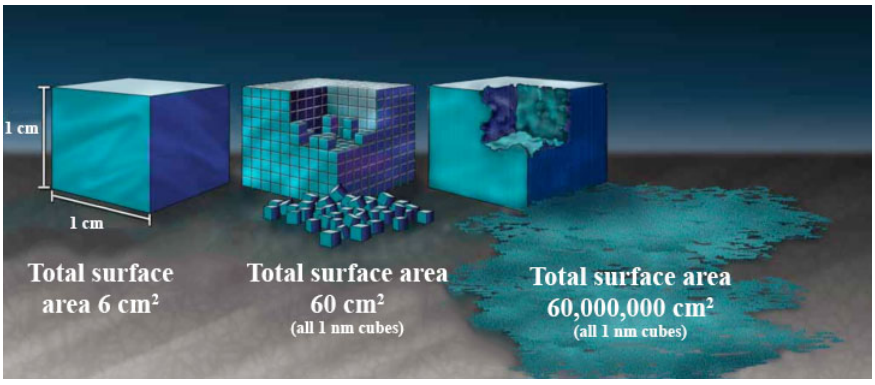

Fig. 2.2: Illustration of the increased surface area provided by nanostructured materials. From ref. [9].

2.2 Classical nucleation theory

Brief overview of a nucleation and a particle growth is stated in this chapter. By the term of nucleation, process of the first–order phase transition is meant. Crossing of the phase boundaries among solid, liquid, and gas is involved. The first order refers to the nucleation and the subsequent particle growth of a nucleus into a bigger structure. Typical examples of these transitions are creation of a rain droplet in the atmosphere or freezing of water into ice crystals [10], [11].

Prerequisite of the nucleation is a stable system. This system needs to be temporarily brought into a thermodynamically unstable state. The nucleation can be consequently defined as the first irreversible formation of a nucleus of the new (equilibrium) phase. The nucleus is a small ensemble of molecules/atoms of the new phase [10]. Nucleation is energy activated process. The growing nucleus is obliged to overcome a free–energy barrier. The nucleus at the top of the barrier determines the nucleation rate which decreases exponentially with the increase of the barrier height. The formation of so called critical nucleus is rather a rare event due to its high free energy which means it has very low probability of forming within a reasonable timescale of the microscopic system.

The nucleation can occur by two distinct mechanisms. The first one is homogeneous which has less frequent appearance. The second one, much more common is addressed as a heterogeneous nucleation and occurs on the interface of nuclei and surface (e.g. impurities of the system). The basic theory describing nucleation and rate R at which nuclei are formed is classical nucleation theory. For homogeneous nucleation, the rate R per unit volume is expressed as the product of an exponential factor and a pre–exponential factor:

$$R = \rho Z j \exp(-\Delta G^*/k_\mathrm{B}T). \tag{2.1}$$

The exponential factor consists of ΔG^* which is the free energy cost of the creation of a critical nucleus, the nucleus at the top of the barrier. The thermal energy is represented by the $k_\mathrm{B}T$ expression. These two factors combined denote the probability of nucleation event occurrence. Generally, the exponential factor emerges from the very low probability of forming the nucleus at the top of the barrier.

The remaining pre–exponential factor is the product of three terms. The number density of molecules ρ, the rate at which molecules attach to the nucleus causing it to grow, j, and the Zeldovich factor. The first term ρ is the number of possible nucleation sites per unit volume. The second one, j, is driven by the diffusion–limited flux onto the nucleus. The final factor is the Zeldovich factor Z which represents the probability that the nucleus at the top of the barrier will continue to form a crystal. It is less than one [11].

The ability to decide whether the nucleation process is slow or fast is important. The $\Delta G(r)$ needs to be calculated for at least approximate estimation of nucleation rate. Classical nucleation theory considers the nucleus as a macroscopic phase. The ΔG is assumed to be the sum of the bulk term which is proportional to the volume of the nucleus, and the surface term, which is proportional to its surface area:

$$\Delta G = \frac{4}{3}\pi r^3 \Delta g + 4\pi r^2 \sigma. \tag{2.2}$$

The first term $\frac{4}{3}\pi r^3$ is volume of a sphere and Δg is related to the chemical potential, thus it is taken as negative. The second term corresponds to the interface at surface of the nucleus, which is the reason why it is surface area of a sphere $4\pi r^2$. σ is the surface tension of the interface between the nucleus and its surroundings, which is positive.

As shown in Fig. 2.3, the interface term $\sim (r^2)$ gives positive free energy and the bulk term $\sim (-r^3)$ gives negative free energy. At some intermediate value of r, the free energy reaches its maximum, and so the probability of formation of the nucleus goes through the minimum.

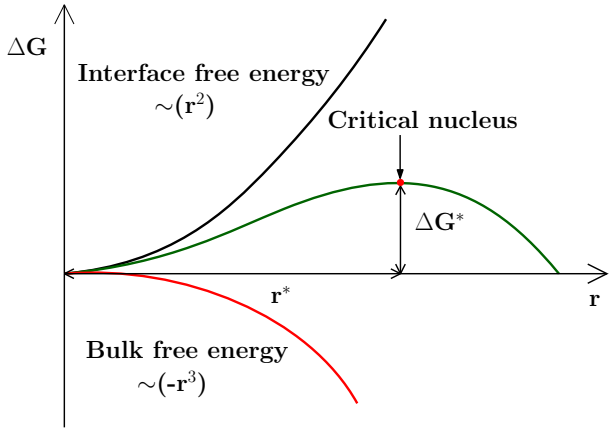

Fig. 2.3: Scheme of the free energy contributions. Inspired by ref. [12].

Critical nucleus is computed by putting:

$$\frac{\mathrm{d}\Delta G}{\mathrm{d}r} = 0. \tag{2.3}$$

This results in the critical nucleus radius:

$$r^* = -\frac{2\sigma}{\Delta g}. \tag{2.4}$$

The final free energy barrier ΔG^* needed, in the classical nucleation theory, to form the critical nucleus is gained by putting r^* into (2.2):

$$\Delta G^*_{\mathrm{HOMO}} = \frac{16\pi\sigma^3}{3(\Delta g)^2}. \tag{2.5}$$

Equation (2.5) gives fundamental relation for the free energy, surface tension, and chemical potential implicated in Δg. By addition of parameters, one can express heterogeneous nucleation on the flat surface as

$$\Delta G^*_{\mathrm{FLAT}} = \Delta G^*_{\mathrm{HOMO}} f(\theta). \tag{2.6}$$

Where θ is the contact angle between the nucleus and the bulk phase [13], [14], [15].

However, calculations of such energies are highly approximate. Therefore, care should be taken with their interpretation. The merit of the nucleation rate lies in its exponential (i.e. Boltzmann factor) factor and related pre–exponential terms.

Along with the nucleus formation the process of particle growth emerges. The process of the particle growth lowers the overall free energy of the system which contains particles and solutes. If there are no competing processes, the growth continues until all of the solute is consumed. Moreover, aggregation of particles also further lowers the free energy of the system, so the particles tend to coagulate and precipitate out of the solution. Therefore, the nanoparticles are obtained only when the reagent is depleted, while the particles are still in the nanometre scope, and when there is no aggregation tendency. Overall, nanoparticles can be stabilised either by electrostatic or steric repulsion. Electrostatic repulsion exploits differences in anions and cations, thus the particles tend to repel one another. The latter uses surfactants as an anti–aggregation agents [16].

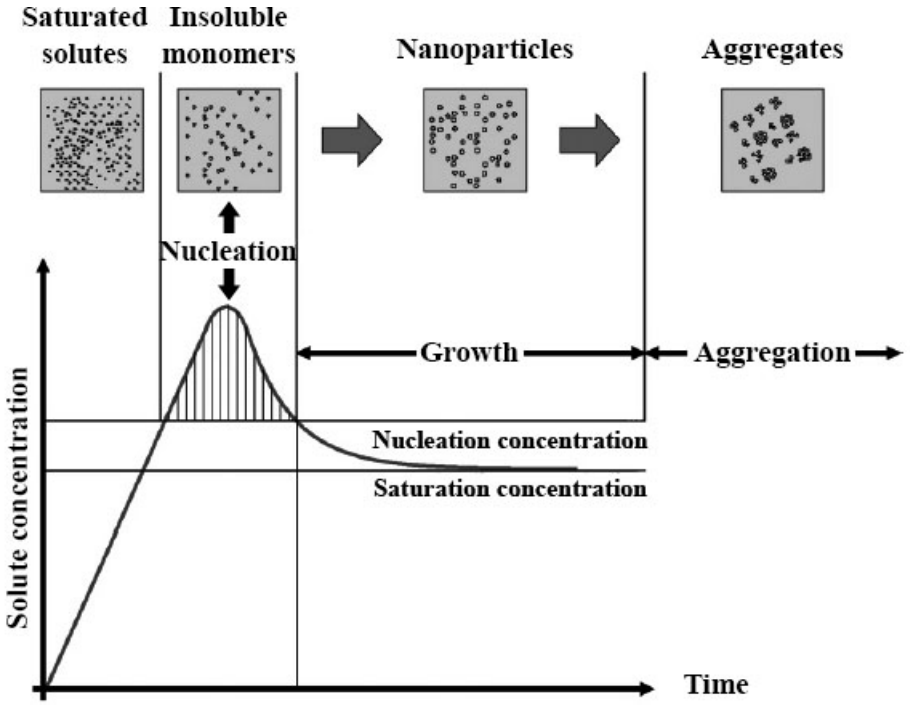

Fig. 2.4: Illustration of nucleation and growth of nanoparticles. From ref. [16].

2.3 Bottom–up approach

As was previously mentioned in the introduction section 1, two general approaches how to produce nanoscale products are distinguished. The most common top–down method is represented by optical or electron beam lithography in the nanoscale. The biggest advantage is its *in situ* applicability, thus no need for assembly step is required. The second method is bottom–up which involves self–assembly. It uses physical and chemical forces in the nanoscale to assemble primitive units into larger structures. This approach is complement to the traditional top–down and its importance arises along with decreasing size of the structures. Inspiration comes from biological systems, which are driven mainly by the chemical forces in the nanoscale [17].

The liquid phase method mentioned later has a major role in the nanoparticles syntheses nowadays. This group of methods can be further sub–divided into liquid/liquid methods, and sedimentation methods.

A typical example of liquid/liquid method is a chemical reduction of metal ions. The reduction method is simple in principle, thus provides facile fabrication of variously shaped nanoparticles, such as nanorods, nanowires, nanoprisms, nanoplates, and hollow structures. Moreover, it is possible to fine–tune the shape and size of the nanoparticles by simply substituting the reducing agent or changing the amount of reductant, the dispersing agent, the reaction time, and the temperature. The process by itself involves reduction of the metal ions to the oxidation state of zero. Another advantage is that demand for equipment is modest. Large quantities of nanoparticles can be yielded by this method in a short time at a reasonable cost. The second branch is addressed as a sedimentation method. In this procedure the general technique is a sol–gel process. This is used extensively for the fabrication of metal oxide nanoparticles.

Chemical synthesis is a route at which nanoparticles of various characteristics can be prepared. Particles are created via self–assembly phenomenon. Significant freedom of the composition of the resulting product is given to a researcher when committing to this preparation procedure. On the contrary, this approach is sensitive to any deviations in preparation conditions and the chance of impurities is increased. The recent trend in syntheses of nanoparticles is to control the particles size, their distribution, shape, and structure. Next step involves improvement of the purity, control of aggregation and subsequent stabilization of physical properties, structures, and reactants in order to maintain feasibility of the procedure. In addition, higher reproducibility, higher mass production at proportionally low costs are matter of a great importance in the nanotechnology industry [1], [18].

2.3.1 Noble metals and metal oxide particles

Overview of interesting noble metals and metal oxide particles is provided. Preparation of metal oxides is often attained by sedimentation. Hydrothermally initiated synthesis and colloidal solutions are still considerable. The importance is in proper selection from diversity of precursors and post–preparation solution treatments such as centrifugation and drying. Main focus is given on noble metals such as gold, silver, palladium, platinum and other metals including cobalt, zinc, copper, and iron. In addition, II–VI metal oxide semiconductor particles preparation techniques are reported as well.

Tab. 2.1: List of substances and final products of noble metals and metal oxides syntheses. Inspired by ref. [19], [20], [21], [22].

Precursors	Products
$ZnCl_2$, KOH, CTAB	ZnO nanorods
$FeCl_2$, $FeCl_3$, NH_4OH	Fe_3O_4 (magnetite)
$CuCl_2$, $ZnCl_2$, NaOH	CuO/ZnO composite
$CoCl_2 \cdot 6H_2O$, $NaBH_4$	Co
Tartaric acid, Ag, Pd, Pt salts	Ag, Pd, Pt
Ascorbic acid, $AgNO_3$	Ag

In Tab. 2.1, shown above, chemical components serving as precursors in noble metals and metal oxides syntheses along with their products are stated. As one can see, precursors are mainly metal chlorides. Reducing agents are often hydroxides and borohydrides with alkali metals such as sodium and potassium. More complex reducing agents including cetyltrimethylammonium bromide (CTAB) and tetraoctyl–ammonium bromide (TOAB) are also frequently used. Particles are prepared by the hydrothermal synthesis. Subsequently, either colloidal solution or supernatant with settled pellet after centrifugation is obtained. These rather non–traditional compounds exhibit interesting structures and properties. For instance Fe_3O_4 has iron cations in two valence states, Fe^{2+} and Fe^{3+}, in the so called inverse spinel structure. Spinel group of magnetite can be expressed as $Fe^{2+}Fe_2^{3+}O_4^{2-}$ [22], [23]. Finally, nanocomposites are generally interesting due to the two component structures, thus potential to exploit the best from each component and the synergy of two–in–one is perceptible.

2.3.2 Syntheses of gold and silver nanoparticles

There are numerous paths in gold nanoparticles (AuNPs) preparation. For instance, Turkevich method [24], Brust–Schiffrin method [25], Perrault method [26], Martin method [27], and other methods. The two firstly mentioned methods date back to 1950s and 1990s, respectively. Remaining methods are quite recent and were developed in the 21st century. AuNPs prepared by the liquid/liquid method are in the form of colloidal solution. This procedure is often addressed as a wet chemistry. Closer look on the original Turkevich et al. method from 1951 and Brust–Schiffrin method is given.

Silver nanoparticles (AgNPs) can be prepared by modified Turkevich synthesis of AuNPs, too. By simple substitution of precursors. The hydrogen tetrachloraurate ($HAuCl_4$) is replaced by the silver nitrate ($AgNO_3$).

Turkevich method

Turkevich in 1951 attained the pioneering experiments in AuNPs synthesis and investigated the effect of the temperature and reagent concentration upon the nanoparticles size and size distribution [24]. In 1973, Frens enriched the method by the description of the control over the size by changing the concentration of sodium citrate, which is the reducing agent. The Turkevich method involves the reduction of gold tetrachloride anion ($AuCl_4^-$) by trisodium citrate ($Na_3C_6H_5O_7$). This reduction is performed by dissolving and boiling of hydrogen tetrachloraurate ($HAuCl_4$) in deionized water. Subsequently, the solution of sodium citrate is added to the boiling gold solution and the heating is carried on for additional dozens of minutes. Change of colour after the addition of sodium citrate is observed. The newly forming solution turns from greyish to dark purple and finally settles into the ruby red colour. The final solution contains gold colloids of approximately 20 nm in diameter. This value fluctuates and is sensitive to the temperature and reagent amount. Typical size deviation is less than 15 %. The biggest advantage of this method lies in its simplicity, mere two precursors plus deionized water are used in the preparation procedure [24], [28].

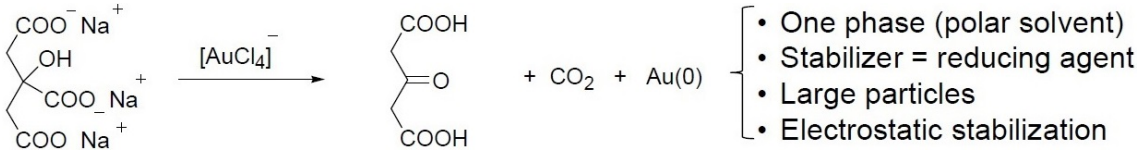

Fig. 2.5: Scheme of Turkevich method synthesis of AuNPs. From ref. [29].

Brust-Schiffrin method

This method was developed by Brust and Schiffrin in 1994. The reaction mechanism is depicted in Fig. 2.6. In the first step, Au(III) ions are reduced to Au(I) by oxidizing alkanethiols (RSH) in order to form Au(I) thiolate complex. The phase transfer of the gold salt from an aqueous phase to an organic phase is attained. The tetraoctylammonium bromide (TOAB) is used as the phase–transfer agent. The second reduction is realized by the addition of sodium borohydride, the main reducing agent. Obtained AuNPs are stabilized in the organic phase by alkanethiol ligands. Moreover, thermal and air stabilization of AuNPs is achieved due to the monodispersed AuNPs being capped by densely packed monolayers. The size of the final particles depends on several aspects such as gold to thiolate ratio, temperature, and the rate at which the reduction is conducted [30], [31], [32].

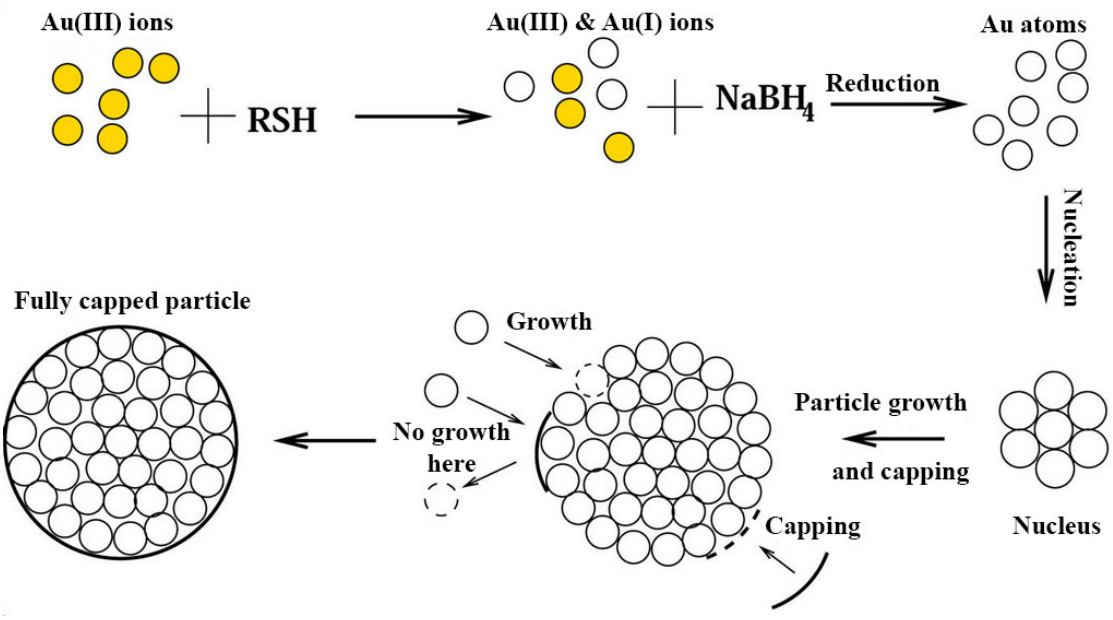

Fig. 2.6: Illustration of mechanism of Brust–Schiffrin method. From ref. [32].

Tab. 2.2: Comparison of Turkevich and Brust–Schiffrin. From ref. [29], [30].

Method	Turkevich	Brust–Schiffrin
Phase	one	two
Reducing agent	citrate	RSH, $NaBH_4$
Stabilizer	citrate	alkanethiol ligands
Particles size [nm]	10–150	1.5–5
Stabilization	electrostatic	steric

2.4 Characterization of nanoparticles

Necessity of the nanoparticles characterization along with several characterization techniques are mentioned in this section. Prepared nanoparticles are subjected to a subsequent analysis in order to qualify and quantify them. The key role in a selection of such a technique is ascribed to the particle size. If one talks about structures in the nanoscale, suitable characterization techniques are relevant. For instance, the particles are rather small for direct optical microscopy imaging. On the contrary, some forms of light scattering used for nanoparticles characterization are not relevant for bigger objects which are sufficiently observed by the optical microscopy [33].

There are numerous and different characterization techniques for various properties. The very first determination, whether nanoparticles are present can be conducted optically. As previously mentioned in the introduction section 1, dichroic appearance of material like Lycurgus cup may indicate presence of nanoparticles. Next method is based on the light scattering by particles in a colloidal solution. This Tyndall scattering effect is called after 19th century physicist John Tyndall [34]. Classical optical microscopy also provides approximate idea of presence of the nanoparticles in a sample. This is caused mainly by the insufficient magnification. Better information about size, morphology, and distribution is reachable by the use of the electron microscopy. Introduction of these characterization techniques that use an electron beam as an information carrier really is a breakthrough. Better understanding of quantum phenomenons along with development of precise engineering in construction of microscopes gave birth to modern era of imaging. Rapid increase in electron microscopy feasibility has allowed a significant progress in the field of nanotechnology since 1950s. Primarily, scanning electron microscopy (SEM) and transmission electron microscopy (TEM) are used. Moreover, atomic force microscopy (AFM) can also be useful in the evaluation of properties of the nanoparticles [35].

Additional techniques such as infrared spectroscopy for composition, zeta potential for estimation of dispersivity, photoluminiscence, absorbance, and surface plasmon resonance for optical properties, and magnetization are representatives of useful characterization techniques. Large amount of available methods can be intriguing, nevertheless, one should always act cautiously and fit the techniques accordingly. The use of relevant physical characterizations after the preparation is crucial nowadays. On the other hand, methods by itself also often have an in–negligible impact on the sample. Therefore, awareness and carefulness when conducting characterization techniques are desirable.

2.4.1 Tyndall scattering effect

This simple method is based on the light scattering by particles in the nanoscale incorporated in the colloidal solution. Realization is not challenging and provides reasonable characterization. Dispersed particles should be in the range of dozens to hundreds of nanometres. When the cross section of particles is near or below the wavelength of visible light, the Tyndall effect occurs [34].

As depicted in Fig. 2.7, two equally filled glasses are prepared. In the first one, on the left side of the picture, a tap water fills the whole glass. The second one contains tap water mixed with a little of semi skimmed milk. If both glasses are exposed to a laser beam, one can see the path of the laser beam in the glass with water mixed with milk. This mixture contains nanoscale particles in the form of fat globules (sub–micrometer size) inherent in the milk [36]. Laser beam is scattered on these particles, and thus is visible by the human eye. In the second glass, laser beam is not visible, scattering does not occur and the beam travels through unheeded by the observer [37].

Use of the Tyndall effect is a great example of convenient characterization technique. The underlying theory explanation may not seem effortless at all, but the practical realization is yet simple.

Fig. 2.7: Tyndall scattering effect. Inspired by ref. [37].

2.4.2 Optical microscopy

Optical microscopy provides the very first view on the sample. The goal of this imaging procedure is to produce magnified visual or photographic image of objects.

The role of optical microscope can be divided into three essential tasks which have to be accomplished in order to get desired output. Optical microscope:

- Produces magnified image of the specimen.
- Is able to distinguish details in the image.
- Renders details visible to the human eye or camera.

Visible light is used to illuminate a sample in the optical microscopy. The usage of wavelengths ranging approximately from 380 nm to 750 nm as an information carrier is a double–edged sword. The sample preparation is quite straightforward and a source of visible light is almost ubiquitous. On the contrary, there are serious limitations mainly in magnification. This is described by the Abbe diffraction limit which practically does not allow an object smaller than half of light wavelength to be observed. Consequently, structures of approximate size of 200 nm and bigger can be seen unspoiled. This gives resultant usable magnification of 1000×.

Another serious problem related to microscopy is the contrast when light passes through very thin sample or reflects from surfaces with high reflectivity. Correction of contrast can be realized by various adjustments including polarized light, phase contrast imaging, differential interference contrast, fluorescence illumination, dark field, and use of optical filters. The basic techniques are bright and dark field microscopy. In the bright field illumination, contrast originates from the absorbance of light in the sample. The contrast in the latter is obtained from light scattered by the sample [38], [39].

Optical microscopy is useful characterization technique. There are recent improvements in this field which cope well with limitations. For instance, the Nobel Prize in Chemistry was awarded to three scientists for "the development of super–resolved fluorescence microscopy" in 2014 [40]. These enhancements help significantly to improve quality and resolution limit of microscope. Another plausible feature is that sample is investigated under ambient conditions. Therefore, the sample can be easily prepared and maintained without any further steps involved which may lead to contamination. However, nanoscale region is not accessible by standard optical microscopy so far. Thus, only for brief examination and detection of the presence of nanoparticles the optical microscopy is suitable.

2.4.3 Scanning electron microscopy

This characterization method has been developed since 1930s. In comparison to optical microscopy, this method perfectly matches requirements for imaging in the nanoscale. A scanning electron microscope (SEM) uses focused beam of electrons to scan a sample. Illustrative scheme of the modern device appearance is depicted in Fig. 2.8 [41].

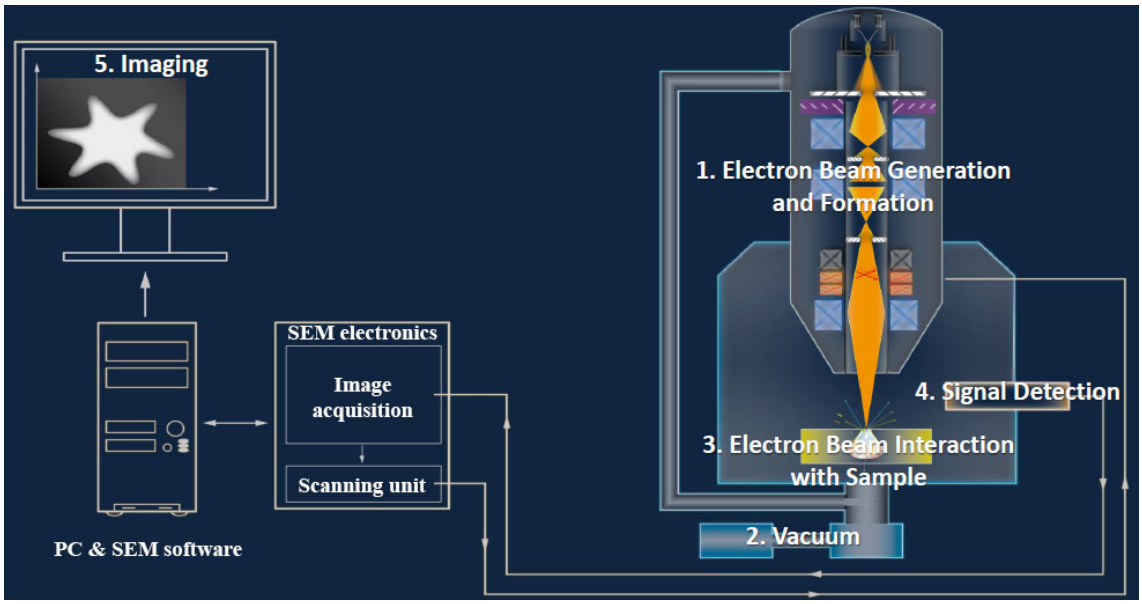

Fig. 2.8: Primary components of modern SEM microscope. From ref. [42].

The first component is an electron source. There are two main groups: thermionic guns and field emission guns. The first group is represented by the tungsten and LaB_6 filament. These sources have larger energy spread, their lifetime is in hundreds of hours and often work in high vacuum region which is roughly from 10^{-3} to 10^{-5} pascals. The latter is represented by field emission Schottky gun. Advantage of this type is lower energy spread and its lifetime is manifold longer than thermionic guns. They usually operate in ultra high vacuum region (i.e. pressure $< 10^{-7}$ pascals) [42].

The next interesting part takes place on the surface of a sample. Interactions leading to several phenomenons happen when electron beam hits the sample. When proper detector is used one can detect various form of information from the sample depending on the electron emission. Secondary electrons are inelastically scattered from the emission of valence electrons. Backscattered electrons are elastically scattered. Therefore, deflections in larger atoms lead to increased collection rate. Auger electrons or X–rays are caused by ejected electrons from the inner shell. Consequently, electron from the higher orbital drops down and fills the vacant energy level [43].

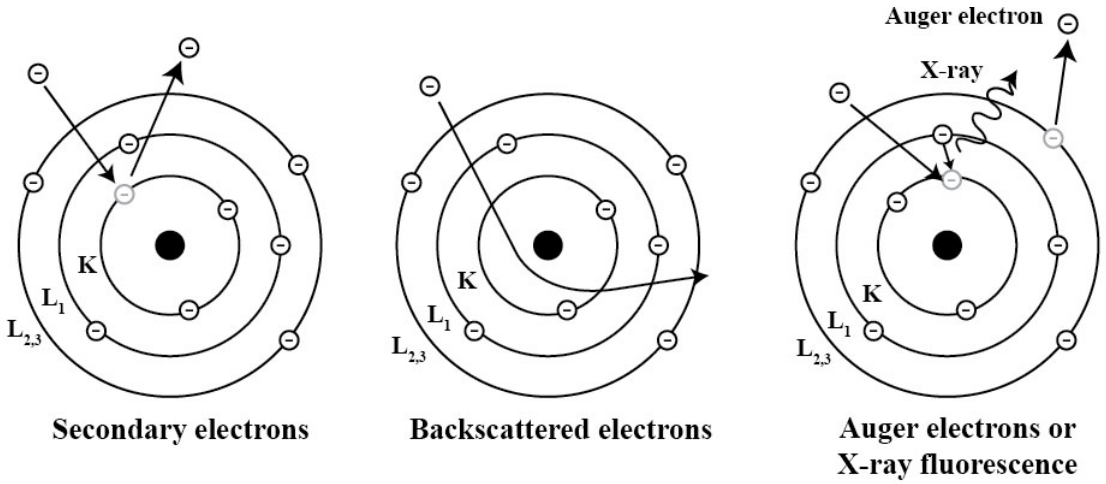

Fig. 2.9: Different modes of electron emission. From ref. [43].

The underlying physical principle lies in the usage of electron beam. Following calculation of electron wavelength is related to the final resolution limit. Considering:

$$\frac{1}{2}m_{\mathrm{e}}v^2 = eU. \tag{2.7}$$

Here one chooses only positive value for speed, although mathematics permits negative value as well. When typical voltage of 30 kV is applied, for an electron one gets:

$$v = \sqrt{\frac{2eU}{m_{\mathrm{e}}}} \doteq 1 \cdot 10^8\,\mathrm{m/s}. \tag{2.8}$$

This speed is close to the speed of light. However, deviation in calculations caused by the special relativity is not remarkable, thus in our simple calculation relativistic correlations are neglected. One can now use wave–particle duality for the electron. By the De Broglie hypothesis:

$$\lambda = \frac{h}{p} = \frac{h}{m_{\mathrm{e}}v} \doteq 0.007\,\mathrm{nm}, \tag{2.9}$$

where h is the Planck constant. This is the result one has been looking for. Unlike optical microscopy, which has maximum resolution of 200 nm, maximum resolution in the SEM is < 1 nm [42]. This is of course theoretical, in the practical usage, there are serious issues to be dealt with. For instance, spherical, chromatic, diffraction, and astigmatism aberrations are all involved. Despite these disturbing elements, SEM is proper characterization device for the nanoscale objects and provides comprehensive examination of sample morphology. The device as itself is versatile and many additional modules can be combined with SEM in order to perform operations in the nanoscale.

2.4.4 Spectroscopy

Absorbance assay measures the intensity of light which passes through a sample. This is realized by input reference cell measurements for each wavelength of incident light. These measurements designate intensity I_0 [W/m^2]. Then, output intensity is measured and denoted as intensity I [W/m^2]. Absorbance A [-] is described by the Lambert–Beer Law:

$$A = \log_{10}\frac{I_0}{I} = \varepsilon l c, \tag{2.10}$$

where ε [dm^2/mol] is molar absorptivity (molar absorption coefficient), l [dm] is length of solution the light passes through, and c [mol/dm^3] is concentration of solution [44].

Photoluminiscece spectroscopy (PL) is a non-contact, non-destructive technique for probing of the electronic structure of materials. In principle, a sample is irradiated by a light. Absorbed light by the sample can induce photo-excitation by which higher electronic state in the material is obtained. This temporary excitation is followed by the consecutive relaxation with spontaneous energy emission. The amount of PL depends on the used material and the laser wavelength [45], [46].

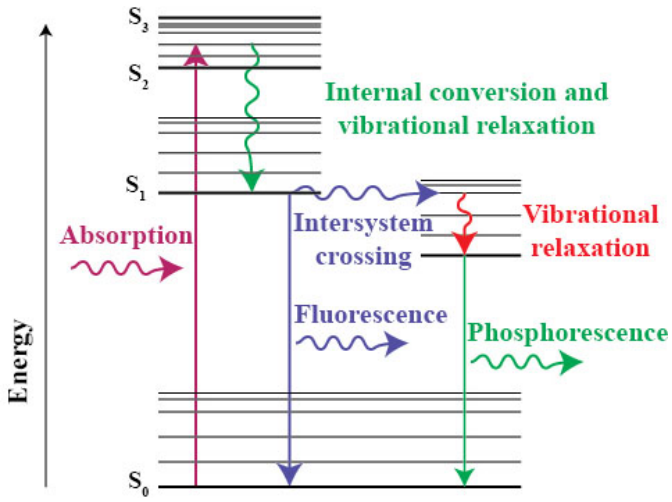

Fig. 2.10: Illustration of absorption/emission of light. From ref. [46].

The quantum yield (QY) of fluorophore represents efficiency of energy transition:

$$\mathrm{QY} = \frac{\text{photons emitted}}{\text{photons absorbed}} = \mathrm{QY}_{\mathrm{ref}}\frac{n^2}{n_{\mathrm{ref}}^2}\frac{I}{A}\frac{A_{\mathrm{ref}}}{I_{\mathrm{ref}}}, \tag{2.11}$$

where $\mathrm{QY}_{\mathrm{ref}}$ is known QY value of a reference fluorophore, n is the refractive index of the solvent, I is the integrated fluorescence intensity, and A is the absorbance at the excitation wavelength [47].

2.5 Applications of nanoparticles

This section provides brief outline of surface plasmon resonance (SPR) phenomenon and overview of possible applications of the nanoparticles. SPR has interesting applicability in sensors. Foremost, gold nanoparticles along with other noble metals and metal oxide particles are mentioned. As referred earlier in the introduction section (1), applications of different nanoparticles in the wide variety of research fields is of a great importance nowadays. This comes hand in hand with the new characterization techniques and better understanding of underlying principles.

2.5.1 Surface plasmon resonance

First observation of surface plasmon resonance (SPR) phenomenon was in 1902 by Wood. Further refinements were given by Lord Rayleigh and Fano. However, complete explanation was not until 1968, when Otto and in the same year Kretschmann and Raether reported the excitation of surface plasmons. Application of SPR–based sensors with biomolecular interaction was firstly provided in 1983 by Liedberg et al. Hereby, basic principle of SPR–based biosensor assay is provided [48].

Term of surface plasmon can be considered as propagating electron density wave occuring at the interface between metal and dielectric. SPR sensing means detection of refractive index changes at the sensor surface which practically infers the amount of mass deposited on the sensor surface. In general, three various optical systems are used to excite plasmons: systems with prism, gratings, and optical waveguides.

The experimental prism set–up depicted in Fig. 2.11 starts with p–polarized light. Incident light is reflected from the inner side of interface between prism and thin metal layer. The metal film acts as a mirror. When changing the angle of light incidence and monitoring the intensity of the reflected light, the intensity of the reflected light passes its minimum. This corresponds to the case of the total reflection, and the reflected photons create an evanescent wave. Therefore, when so called resonance angle is achieved, the light excites surface plasmons and induces SPR, thus the dip in the intensity of reflected light occurs. Photons of p–polarized light are able to interact with the free electrons of the metal layer. They cause a wave–like oscillations of the free electrons. Consequently, reducing the intensity of the reflected light.

Moreover, the sensorgram is depicted below the set–up. The SPR angle shifts (from I to II, left side of the diagram) when biomolecules bind to the surface and therefore change the mass. This change in resonant angle can be monitored in real time and plotted as a resonance signal (proportional to mass change) versus time (right side of the diagram) [48], [49], [50].

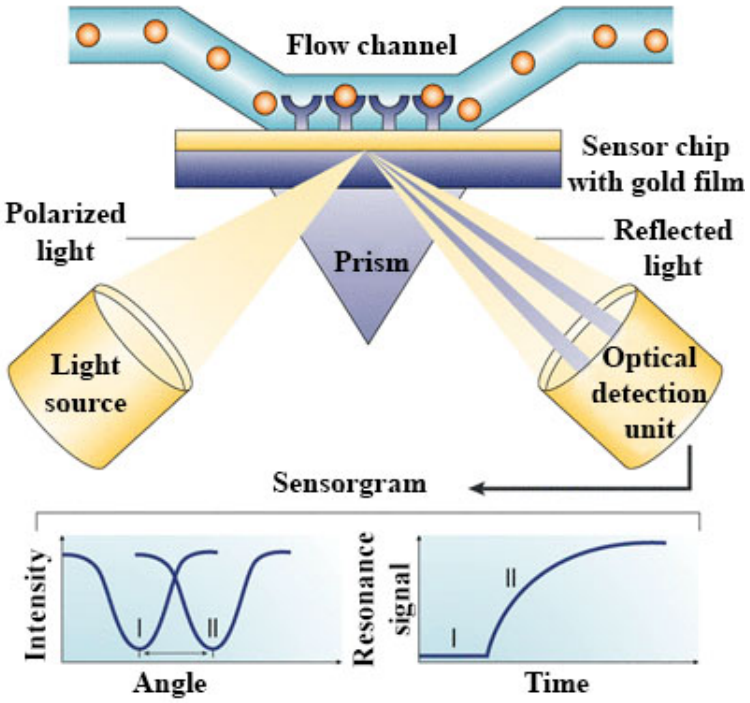

Fig. 2.11: Diagram of Kretschmann configuration of SPR–based sensor. From ref. [50].

SPR and metal nanoparticles

SPR is not restricted to planar multilayers. Instead, metal nanoparticles can exhibit SP effects at the greater extent. Generally, the net electric field in the vicinity of dielectric particle is the superposition of the external applied field and the induced (dipole) field in the particle. By choosing the angular frequency that excites plasmons in the metal and detecting scattering frequencies, both the excitation and the scattered field are enhanced by the presence of the metal particle. This is used in the surface–enhanced Raman spectroscopy (SERS) which provides immensely enhanced signals. Thus, enormous sensitivity is obtained and SERS can detect single molecules. Along with its high molecular specificity, detection of low concentrations of biomolecules such as DNA strands or proteins can be achieved. In addition, these field enhancements might also be useful in the detection of fluorescent molecules near metal nanoparticle. Consequently, metal nanoparticles are considered as surface plasmon–assisted field amplifiers [48].

SPR also elucidates the ruby red appearance of colloidal AuNPs. For instance, wavelength of the SPR band maximum of a spherical AuNP is $\sim 520\,\text{nm}$. If colloidal AuNPs solution is irradiated by the visible light at these wavelengths, the visible green light is absorbed while red light $\sim 700\,\text{nm}$ is reflected. This effect gives the AuNPs the ruby red appearance [1], [51].

2.5.2 Particular applications

Metallic nanoparticles have fascinated scientist for decades. Nowadays, they are heavily utilized in both biomedical sciences and engineering. Their huge potential lies especially in nanotechnology. These materials can be synthesized and modified with various functional groups. This allows them to be conjugated with antibodies, ligands, and drugs. Therefore, wide range of applicability is in biotechnology, magnetic separation, targeted drug delivery, and diagnostic imaging. Many imaging techniques have been developed over the years such as MRI, CT, PET, ultrasound, SERS, and optical imaging. They all aid to image various disease states [52].

Moreover, nanoparticles may be involved in the treatment of cancer by using hyperthermia which refers to the increasing temperature within the human body. Temperature of the human body is normally slightly above 36 °C. Increase of mere 6 °C to 42 °C significantly reduces viability of living cells which ultimately causes death. In hyperthermia therapy, nanoparticles are selectively bonded to cancerous cells and consecutively exposed to an external stimuli. External energy source can be realized by alternating current magnetic field, an intense light source or radio frequencies. NPs are heated up and induce thermal ablation of the tumour. The first *in vivo* Phase II clinical trials (i.e. 100–300 people are tested [53]) were realized by magnetite nanoparticles in Germany in 2005. Tests were successful and results showed the ablation of the tumour after several sessions with no significant collateral tissue impairments.

Gold nanoparticles

AuNPs have proven to be suitable drug carriers and gene delivery agents. The task is to fully control binding, transportation, and release of drugs in the requested site. The release can be initiated either by internal (e.g. pH) or external (e.g. light) stimuli. Advantages of AuNPs usage are following: gold cores are considered to be non–toxic and inert, modesty of synthesis, and versatile functionalization potential which is mainly provided by thiol linkages. Typical link stabilizers are oligo(ethylene glycol) and poly(ethylene glycol). These attachments to biomolecules decrease probability of non–specific adsorption of other unwanted molecules [54].

AuNPs can also be used in the cancer therapy. The first step is tumour targeting. This can be conducted with previously mentioned surface functionalized NPs with antibodies, peptides, and/or DNA/RNA to specifically target cellular receptors. Moreover, AuNPs can be attached to a single–stranded oligodeoxy–nucleotides for gene therapy as regulators. AuNPs are also relevant for biosensors (e.g. SPR–based 2.5.1). Most therapeutic and imaging methods rely on AuNPs, mostly due to their low toxicity and convenient preparation [55].

Silver nanoparticles

Among many fields of silver nanoparticles applications such as catalysts, optical sensors, and electronics, the most desired medical field stands out. The biggest advantage and drawback at the same time lies in the small size of particles. Nanoparticles are even able to cross blood–brain barrier, which could be useful in drug delivery. However, such applications are still far from the safe realization. Another article [56] also mentions bactericide ability of the silver nanoparticles. Therefore, it is more likely to use them incorporated in fabrics as wound healing supporters. Toxicity of silver ions and silver–based compounds to bacteria is ascribed to the ability of silver to anchor to the bacterial cell and subsequently penetrate it. Sulfur–containing proteins are abundant on the bacterial cell membrane. Thus, silver nanoparticles can interact with these proteins either from the inside or from the outside of the cell membrane. This causes changes in the cell membrane structure which mean nothing but a death of the cell itself. Presented mechanism is based on the theory of hard and soft acids and bases [57]. Silver is considered as a soft acid. On the contrary, sulfur and phosphorous are considered to be soft bases. Therefore, natural tendency to react occurs.

For instance, nanosilver–based wound dressing was presented in 1995 and is sold as Acticoat nowadays. Dressings in this manner could prove useful in treating burnt patients suffering from the toxic shock syndrome. They could also be beneficial in the bone cements as artificial joint replacements and in the silver nanoparticle–coated propylene mesh as the surgical antimicrobial mesh [56].

Potential of Ag nano–coated cotton fabric as an antiseptic dressing or bandage was demonstrated by Lee and co–workers [58]. Based on their experiment, they concluded that the silver nanocoated fabrics exhibit bactericidal activity depending on the dose of nanoparticles. Bactericidal effect varies according to different bacteria type (gram–positive/gram–negative strain with/without antibiotic resistance). Potential of this fabric as an antiseptic bandage was validated. It is promising fabric for the medical treatment of skin burns or cuts.

All these applications should be taken cautiously. Silver nanoparticles are highly toxic and harmful to people and environment when treated inadequately [56].

ZnO

Nowadays, the majority of ZnO production is used is rubber and concrete industry. ZnO aids in vulcanization process where it improves heat conductivity. This is useful in heat dissipation when the tyres roll. In concrete industry, admixture of ZnO improves the resistance of concrete against water. Due to its wide direct gap (3.4 eV), ZnO is transparent in the visible electromagnetic spectrum. Therefore, it can be used as a transparent conducting oxide. This could be beneficial as the front contact for solar cells, front contact of liquid crystal displays or in the production of energy–saving or heat–protecting windows [59].

Other current applications concern mainly medicine, ceramics, animal feed, lubricants, paints, catalysts, and cosmetics. ZnO is contained in suntan lotions where it serves as an UV–blocker as well [60].

Forthcoming applications can be represented for instance by the gas sensors. This utilization emerges from the ability that ZnO surface conductivity can be influenced by various gases. Moreover, some of the field–effect transistors use ZnO nanorods as conducting channels [59].

CuO/ZnO composite

Application of this composite in waste water treatment was recently presented [61]. Photocatalytic properties were evaluated by photodegradation of methylene blue (MB) and methylene orange (MO) under UV irradiation. It was observed that MB and MO can be degraded within 15 and 25 min by this CuO/ZnO composite and photodegradation is 6 times faster than by pure ZnO. Moreover, increase of CuO phase can improve the photocatalytic efficiency of the composite. This enhancement of photocatalytic activity could be ascribed to the low recombination probability of photo–induced carriers due to the efficient charge transfer in the composites.

This composite can also be beneficial in biological applications [21]. It could serve as selective cystein (Cys) and homocystein (Hcy) detector. The presence of Cys and Hcy in the solution induced colour change from light blue to dark grey. All proteinogenic amino acids were subjected to this test and were mixed with prepared solution. However, just in the case of Cys and Hcy the colour change occurred and was visible by the human eye. The assay method is based on the reduction of Cu(II) to Cu(0) in the presence of Cys and Hcy. This process leads to 75 nm–blue shift of the peak located in the absorption spectrum at 725 nm.

3 EXPERIMENT

Motivation for this part was to provide step-by-step guide for preparation, deposition on substrate, and characterization of nanoparticles. Prepared structures were in the form of a colloidal solution or had powder–like appearance. Standard silicon wafers were cut to pieces. They were meant to fit SEM stage, thus optimal dimensions were about 7×7 mm. Afterwards, drop casting method and consecutive evaporation were conducted. Evaporated sample on the silicon substrate can be further subjected to the optical or electron microscopy. Both characterizations served to determine morphology of observed specimen. Hereby prepared structures can be further processed and incorporated in applications as mentioned in the section 2.5. However, direct applications with detail analyses were not carried out in this thesis. Instead, influences of external (i.e. ambient conditions) and internal factors (e.g. compound concentrations and ratios) on the final structure were introduced.

Calculation of precise components weight preceded every preparation. Weight calculations within experimental section were given by equation (3.3). Amount of component is often expressed by molar concentration c [$1\,\mathrm{mol/dm^3} = 1\,\mathrm{M}$] and volume V [$1\,\mathrm{dm^3} = 1\,\mathrm{l}$]:

$$c = \frac{n}{V}. \tag{3.1}$$

Required mass m [1 kg] is featured in the mole n [1 mol] expression:

$$n = \frac{m}{M_\mathrm{m}}. \tag{3.2}$$

Combining these two equations and expressing for m gives:

$$m = cVM_\mathrm{m}, \tag{3.3}$$

where M_m [kg/mol] denotes molar mass.

Laboratory preparations and syntheses were carried out at the room temperature and pressure (temperature of 25 °C and pressure of 101.325 kPa). All weighing was performed on the analytical scales Scaltec SBA 31. Substrate preparations, drop castings, and microscopy observations were carried out in clean room (class $<$ 100 000) located at the Institute of Physical Engineering, Faculty of Mechanical Engineering, Brno University of Technology. Characterization of size and morphology of samples has been performed by optical microscope (Olympus MX51) and scanning electron microscope (TESCAN LYRA3 XMH and TESCAN VEGA). Absorption and fluorescence measurements were performed by UV–Vis spectrophotometer (Jasco V-630) and spectrofluorometer (FluoroMax–4 HORIBA Jobin Yvon), respectively. Samples were measured at the Department of Biophysics of Slovak Academy of Science in Kosice by RNDr. Michaela Šimšíková, Ph.D.

3.1 Gold nanoparticles

Overall, several AuNPs syntheses were carried out. Hereby, the next section represents the preparation of gold spheres using Turkevich method and gold rods prepared by the seed solution method.

3.1.1 Spheres

Gold spheres were prepared by adaptation of Turkevich method [62]. First of all, 2 ml of solution containing 17.26 mg $HAuCl_4 \cdot 3H_2O$ was diluted in 200 ml of deionized water (DW). This solution was vigorously stirred and brought to boil. Afterwards, 12 ml solution containing 106.8 mg trisodium citrate dihydrate (TC) was added to the boiling solution. Mixture was boiled for additional 30 minutes. After this time period, the mixture was put aside from the hot plate and let to cool down to the room temperature. Prepared colloidal solution was poured over to centrifuge tube and stored in the dark.

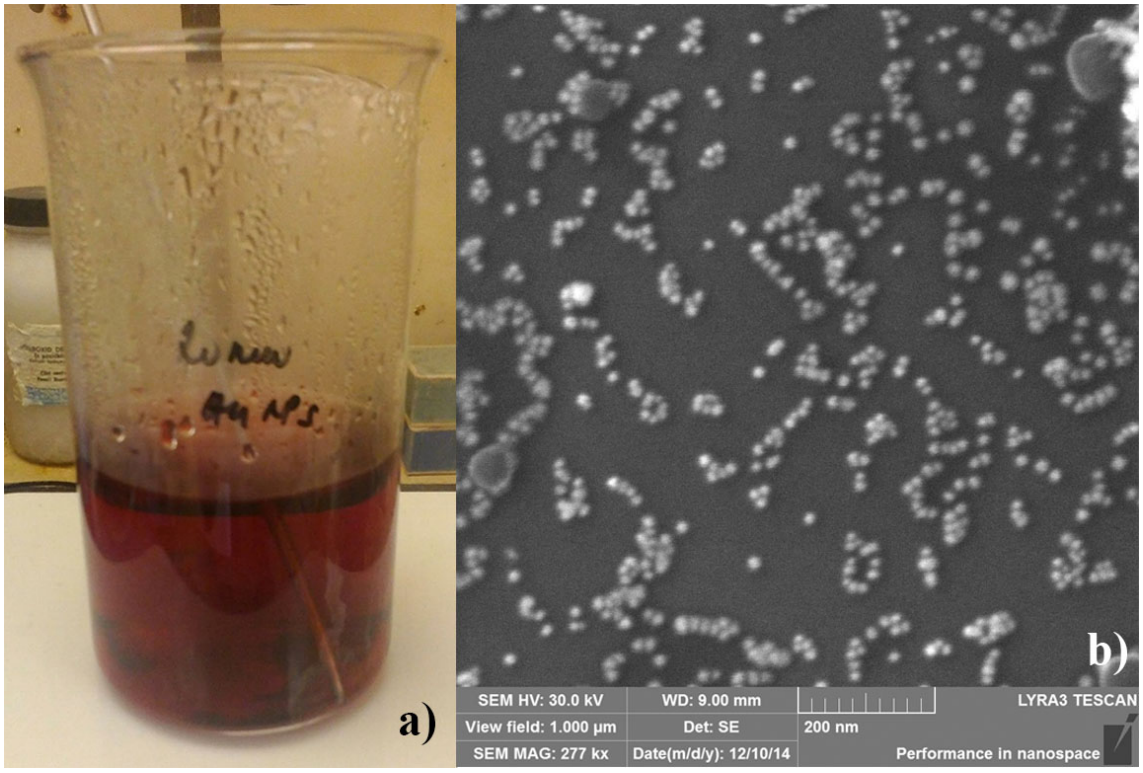

Fig. 3.1: SEM images: a) red appearance of AuNPs during the synthesis, b) image of gold spheres. Spherically shaped AuNPs with average diameter of 20 nm. Particles are locally aggregated.

Another sample of AuNPs was prepared by Turkevich method as well. However, the ratio of reactants has been change during the preparation process. Firstly, 10.6 mg $HAuCl_4 \cdot 3H_2O$ was diluted in 100 ml of DW. This solution was vigorously stirred and brought to boil. Afterwards, 6 ml solution containing 30.3 mg TC was added to the boiling solution. Mixture was boiled for additional 30 minutes. After this time period, the mixture was put aside from the hot plate and let to cool down to the room temperature. Prepared colloidal solution was poured over to centrifuge tube and stored in the dark.

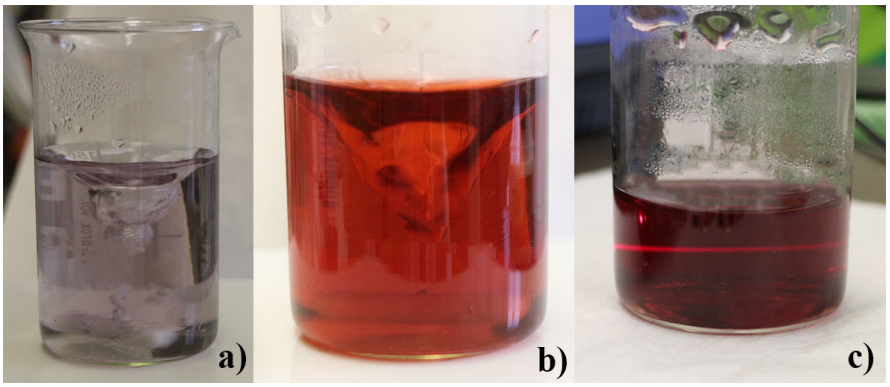

Fig. 3.2: Images from preparation: a) start of the nucleation right after addition of TC, b) nucleation and growth in progress, red-dish colour starts to take over, c) Tyndall scattering effect on prepared ruby red particles.

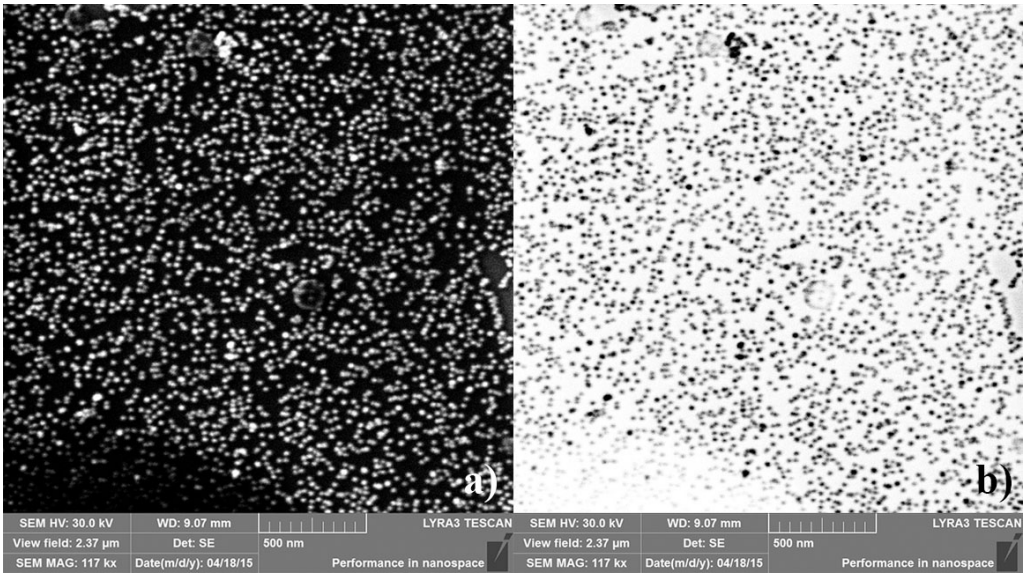

Fig. 3.3: SEM images of gold spheres from the second sample: a) spherically shaped prepared AuNPs with average diameter of 20 nm. Particles are modestly aggregated, b) the same SEM image with inverted colours.

3.1.2 Rods

Gold rods were obtained by three-step one phase reaction [63].

First step involves synthesis of seed solution. Thus, 0.25 ml of solution containing 0.985 mg $HAuCl_4 \cdot 3H_2O$ was added to 7.5 ml of solution containing 273.3 mg TC in a test tube. Subsequently, 0.6 ml solution containing 2.27 mg $NaBH_4$ was mixed into the same test tube.

In the second step, growth solution containing a mixture of CTAB solution (173.11 mg CTAB, 4.75 ml DW), $HAuCl_4 \cdot 3H_2O$ solution (0.788 mg, 0.2 ml DW, and $AgNO_3$ solution (0.05 g, 0.03 ml DW) was prepared. At last, 0.032 ml solution containing 0.564 mg ascorbic acid was added to the growth solution.

Finally, 0.01 ml of seed solution gained in the first step was added to the solution gained in the second step. Resulting mixture was gently mixed and left undisturbed.

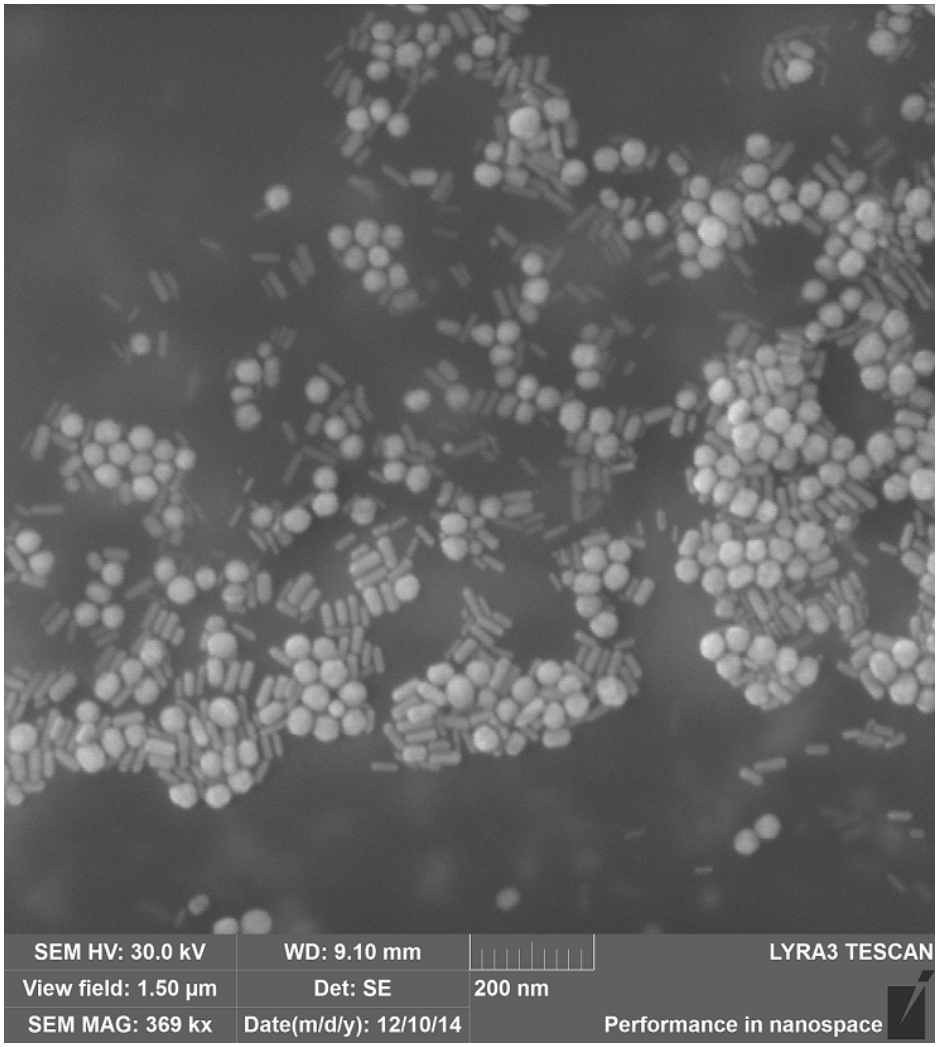

Fig. 3.4: SEM image of gold rods. Rods are approximately 60×20 nm in cross section. Particles are locally aggregated. Apparent cobblestone-shaped impurities.

3.2 Silver nanoparticles

AgNPs were prepared by modified synthesis of AuNPs [64]. Four solutions were prepared. Each solution contained 4 mg $AgNO_3$ diluted in 40 ml of DW. These mixtures were vigorously stirred and brought to boil by the hot plate. As soon as mixtures boiled, different amount of TC was added to the boiling solutions. Subsequently, boiling was sustained for additional 10 minutes. After this time period, the mixture was put aside from the hot plate and let to cool down to the room temperature. Prepared colloidal solutions were poured over to centrifuge tubes and stored in the dark.

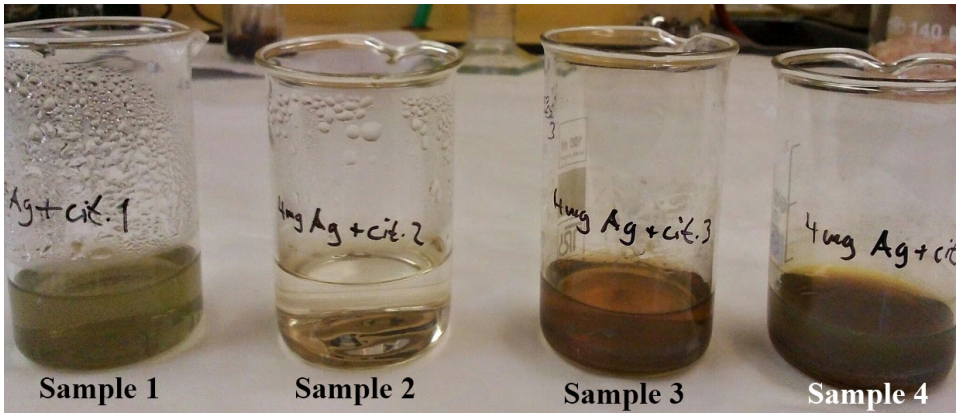

Fig. 3.5: Prepared AgNPs samples: 1) 4 mg Ag + 181.17 mg TC, 2) 4 mg Ag + 20.47 mg TC, 3) 4 mg Ag + 20 mg TC, 4) 4 mg Ag + 18.12 mg TC.

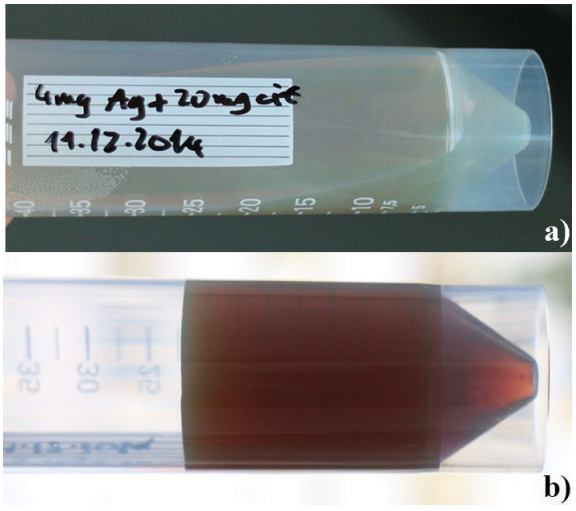

Fig. 3.6: Dichroism effect on the prepared AgNPs: a) particles are lit from the front and appear green, b) particles are lit from behind, through the window in this case and appear red instead.

The third sample of prepared AgNPs (4 mg Ag + 20 mg TC) has been later deposited onto a substrate. Particles were deposited on Si (100) conductive wafer by drop casting method with consecutive evaporation. Temperature of hot plate during the evaporation was set to 60 °C in order to support evaporation speed. This method leads to ready samples for the optical and electron microscopy.

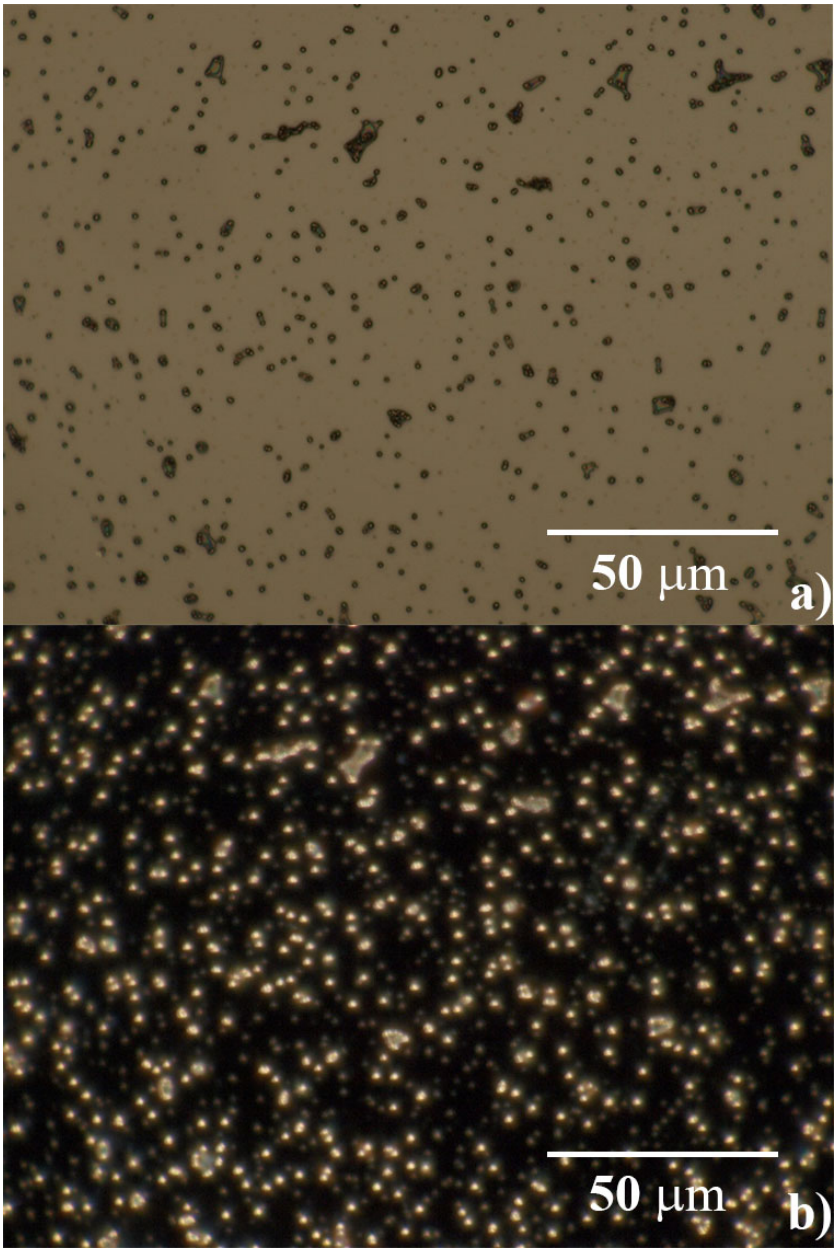

Fig. 3.7: Images from the optical microscope: a) bright field microscopy, b) dark field microscopy. Field of view: 180 µm.

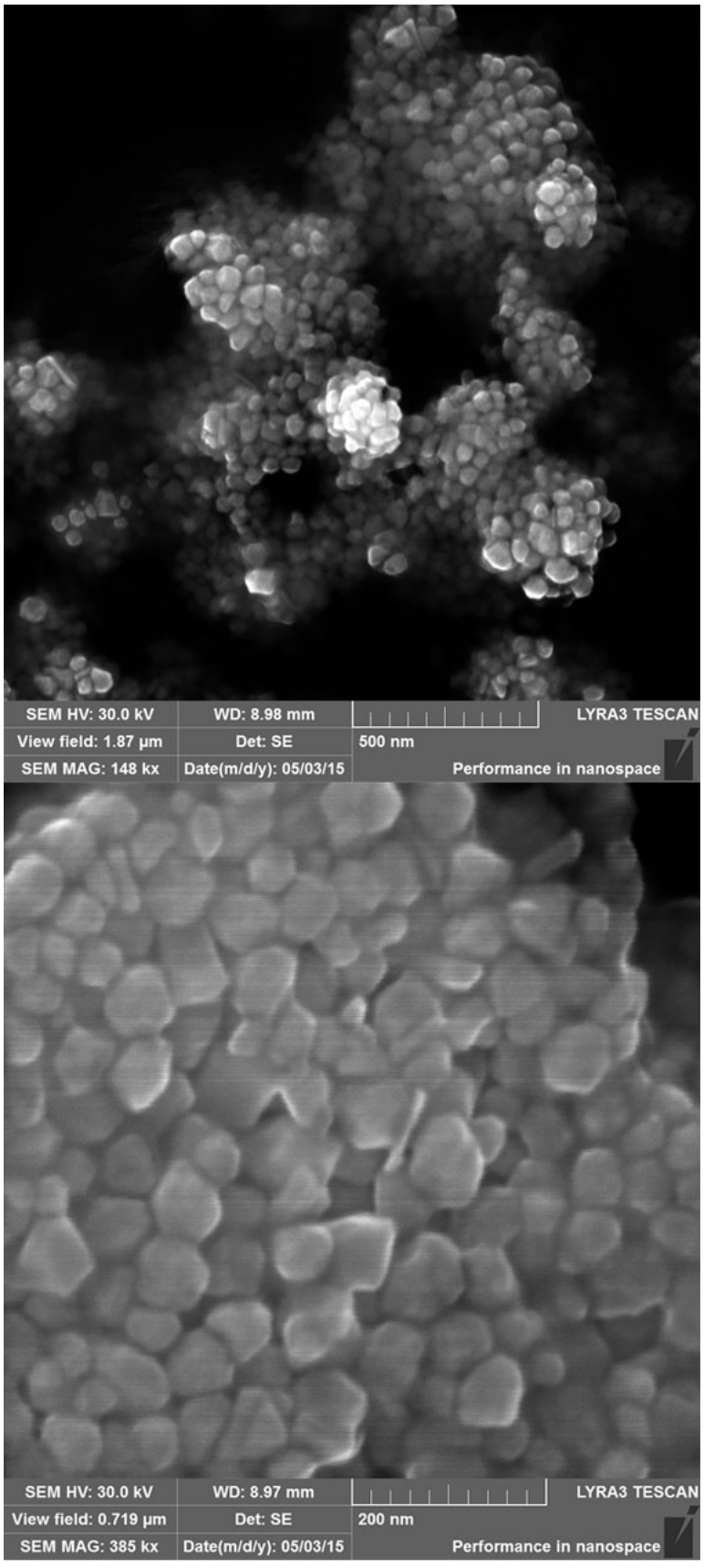

Fig. 3.8: SEM images of prepared AgNPs in the form of cobblestones with the size ranging approximately from 30 nm to 80 nm.

3.3 ZnO

ZnO nanoparticles were prepared by modified synthesis mentioned by NI and co–workers [19]. Firstly, 10 ml solution containing 1.363 g $ZnCl_2$ was added to a beaker. Secondly, 10 ml solution containing 1.121 g KOH was added to the same beaker. This mixture was completed by adding 10 ml solution of 1.822 g CTAB. Final solution was vigorously stirred and brought to boil. Mixture was boiled during 30 minutes. Prepared colloidal solution was dried at 120 °C during 120 minutes.

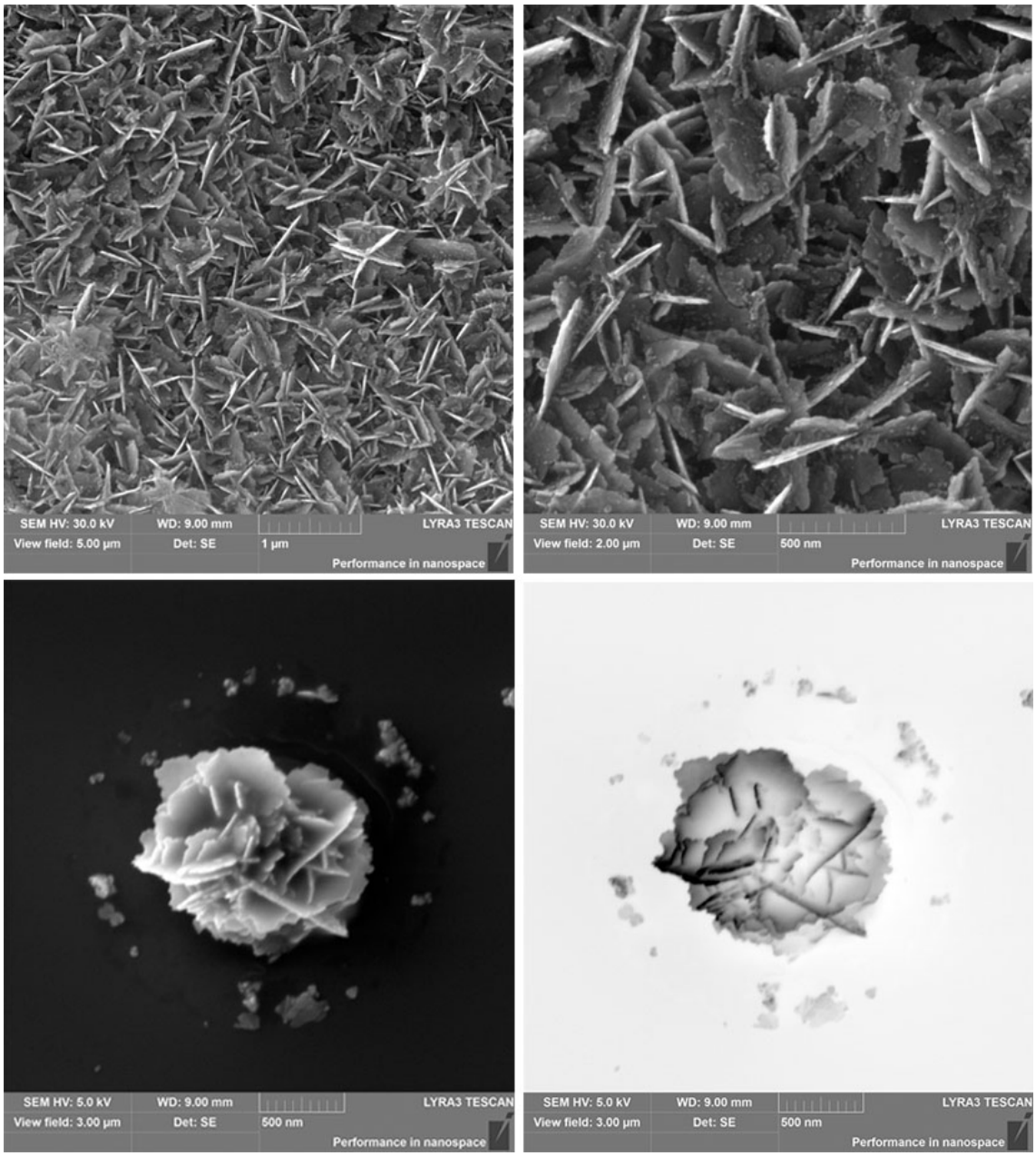

Fig. 3.9: SEM images of ZnO nanoplates and nanoflowers.

3.4 CuO/ZnO composite

CuO/ZnO composites at various ratios of starting reagents have been prepared. Every solution contained 2.017 g of $CuCl_2$ dispersed in 75 ml of DW. Subsequently, 75 ml solution containing appropriate amount of $ZnCl_2$ to form desired ratios was added to the $CuCl_2$ solution.

Tab. 3.1: Amount of $ZnCl_2$ needed to add to the $CuCl_2$ solution.

$CuCl_2$:$ZnCl_2$	9:1	6:1	3:1	1:1	1:3	1:6	1:9
$ZnCl_2$ [g]	0.225	0.341	0.681	2.045	6.134	12.267	18.401

Solutions were mixed for 2 minutes. Afterwards, mixed solutions were added to 187.5 ml solution containing 1.5 g NaOH. Mixtures were vigorously stirred and boiled on the hot plates.

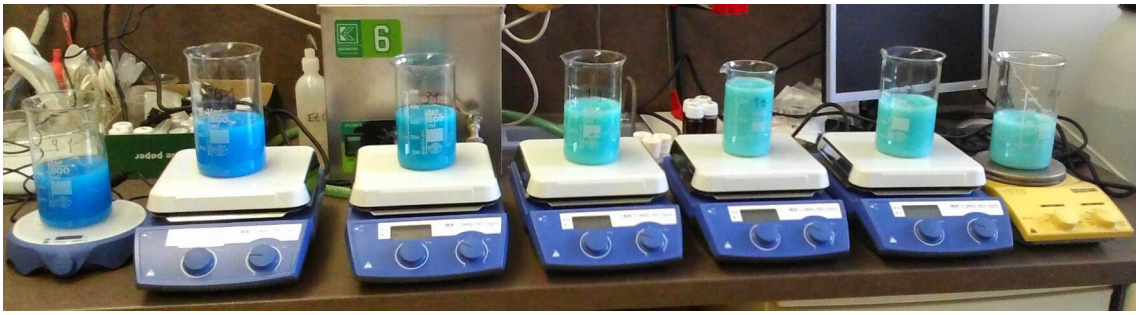

Fig. 3.10: Prepared CuO/ZnO solutions of different ratios. From the left to the right: 9:1, 6:1, 3:1, 1:1, 1:3, 1:6, and 1:9 of CuO:ZnO.

Subsequently, prepared samples were washed in DW and collected through centrifugation (Heraeus Megafuge 40 Centrifuge). This process was repeated several times until the neutral pH of supernatant was obtained. Finally, solutions were dried at the room temperature.

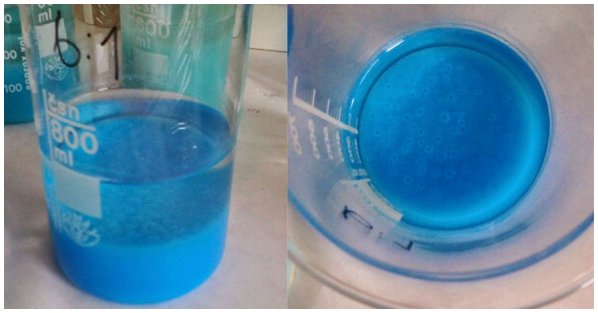

Fig. 3.11: CuO/ZnO sediment of 6:1 ratio.

Fluorescence emission spectra exhibit UV band around 386–409 nm and another emission band in the visible spectra at 720–754 nm which is in the vicinity of near infrared spectrum. Peak in the UV region corresponds to the recombination of electrons in the conduction band and holes in the valence band. Consequently, visible emission is caused by the presence of impurities and structural defects such as oxygen vacancies or interstitial oxygen. Absorption spectrum exhibits well-defined peak in the visible spectra. Slight shift in the absorption peak and change of its shape can be achieved by the change of ratios of Cu and Zn in the prepared material.

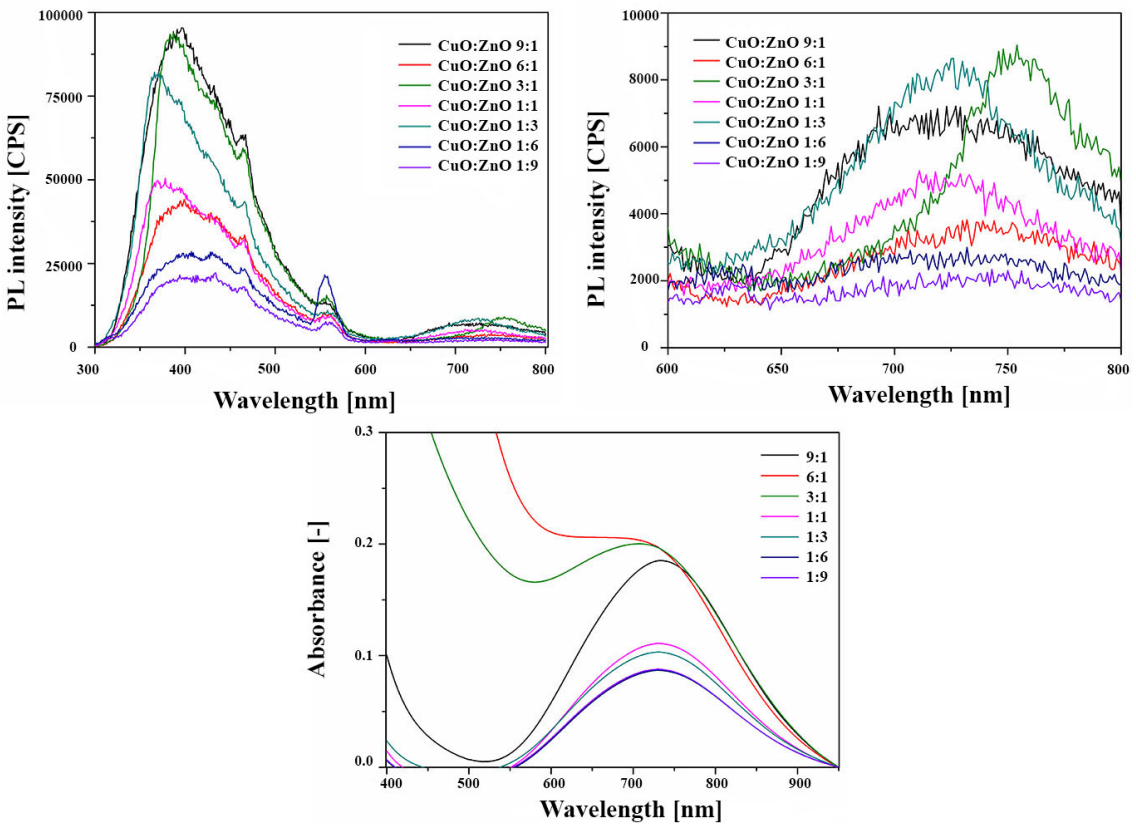

Fig. 3.12: Photoluminiscence and absorbance of CuO/ZnO.

The morphology of the prepared materials was studied by SEM. The results indicate that the ratio of the metals in the composite has a significant impact on the size and structure of the material. CuO/ZnO composite forms needles, quasi spheres, and hexagonal plates when the ratio is 3:1, 1:1, and 1:3, respectively. Images are shown on the next page in Fig. 3.13.

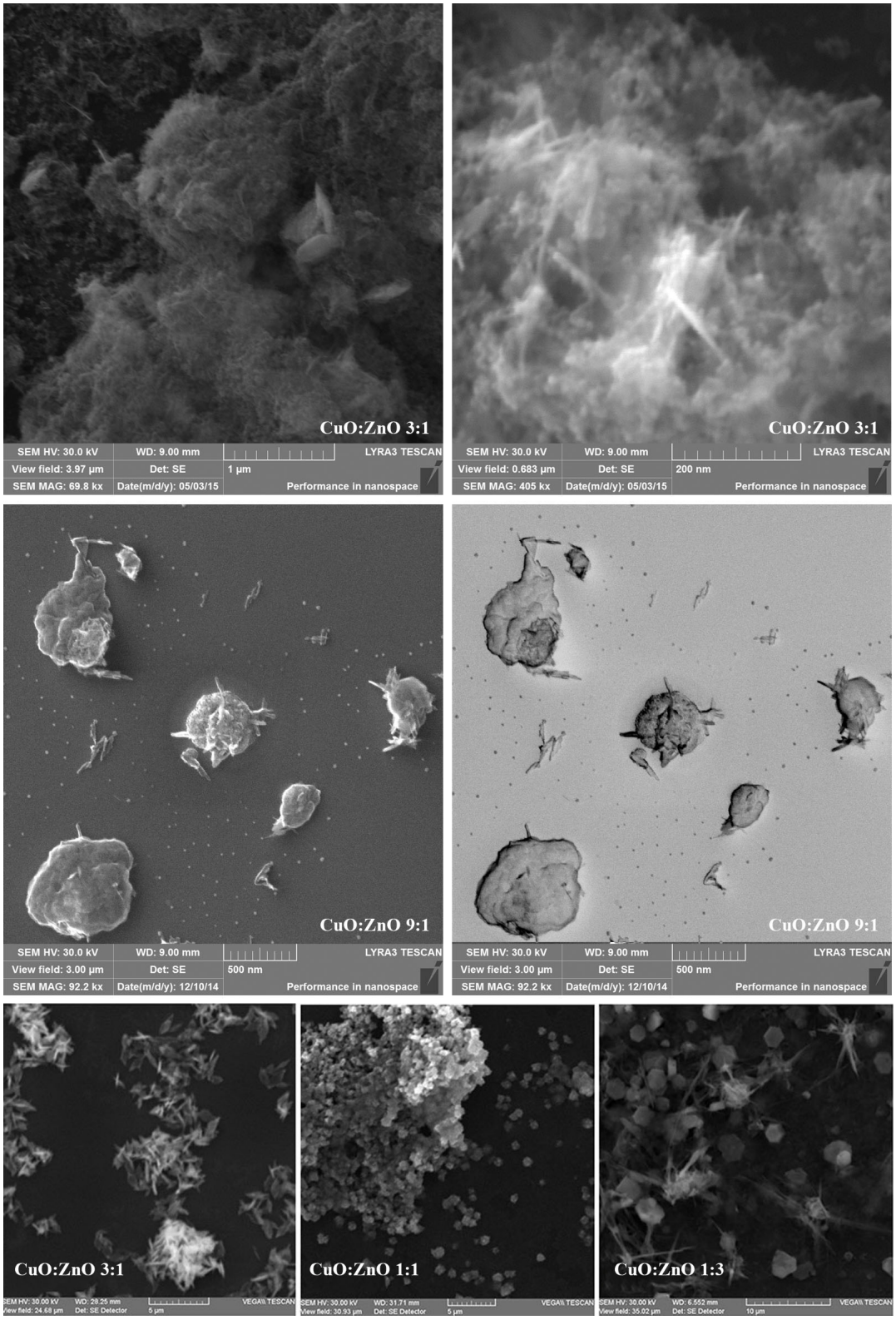

Fig. 3.13: SEM images of CuO/ZnO composite.

4 CONCLUSIONS

This section evaluates results and briefly discusses remarks which accumulated during experiments. This thesis demonstrated hydrothermally initiated syntheses of nanostructures by the bottom–up method with consecutive characterization and outlined possible applications. Goals of thesis were carried out in successive steps. This involved theoretical background for preparation, characterization, and application of nanostructures. Subsequently, experimental part demonstrated preparation of variously shaped nanostructures. Selected nanostructures were prepared and characterized with reasonable quality. This was demonstrated mainly by the SEM images of structures. Additional characterization methods help to imagine general morphology and properties of structures.

Inceptive step of the preparation is quite straightforward. However, small masses of weighted compounds represent an issue. Furthermore, compound constituting gold nanoparticles $HAuCl_4 \cdot 3H_2O$ has proven to be very hygroscopic, thus one has to be swift during manipulation with it. Syntheses by itself are influenced by the compounds concentrations, ambient conditions, and ubiquitous impurities within all steps: preparation, storing, deposition, and observation. Moreover, uniformity of particles deposited on the silicon substrate while using the simple drop casting method is not satisfactory.

Characterization by the optical microscope is not sufficient in the nanoscale and serves only for the approximate estimation of morphology. This is the reason why only images for silver nanoparticles were published. Nevertheless, SEM seems to be plausible characterization method. Slight issue is with charging of particles during the observations. Choice of detector is also matter of a concern. All images were acquired by using secondary electrons (SE) detector. Instead, use of scanning transmission electron microscopy detector (STEM) is considerable and subject of further studies.

Two samples of golden nanospheres were prepared (3.1.1). Both correspond to the Turkevich preparation method. Average diameter of particles for both samples is 20 nm. Rods were prepared by the seed solution method (3.1.2). The sample with rods also contained gold spheres which can be attributed to the impurities and deviations in the concentrations within the preparation. The particles are locally aggregated. Moreover, overall particles aggregation becomes more significant over time. The impurities involved during all steps: preparation, storage, deposition, and observation play considerable role.

Silver cobblestones were prepared by the modified Turkevich synthesis (3.2). The sample exhibits spatially uniform flocculates formed over time as solution idles. Size of cobblestones spans from 30 nm to 80 nm.

Zinc oxide nanostructure have been prepared by the chemical precipitation method (3.3). Zinc oxide plates and flowers exhibit wurtzite crystal structure. This sample represents the II–VI semiconductor structure.

Copper oxide – zinc oxide composite samples were prepared at the different ratios of compounds (3.4). Selected samples were also subjected to SEM. Resulting morphology consists of hexagonal spheres, plates, and needles. Structure is dependant on the concentration of compounds. Photoluminiscence along with absorbance represent
measurements of optical properties which can also be altered by the change of ratios of compounds.

The aim of this study was to provide simple yet compact practical guide through the structures in the nanoscale. Although thesis tries to cover and provide full experience of topic, every step presents opportunity of improvement, enrichment, and is subjected to further investigation. Particular applications of particles in the nanoscale were described in the theoretical section. Some of described applications will be studied on the prepared nanostructures in the upcoming diploma thesis.

BIBLIOGRAPHY

[1] HORIKOSHI, Satoshi and Nick SERPONE. *Microwaves in nanoparticle synthesis: fundamentals and applications*. Weinheim: Wiley-VCH, 2013, xv, 332 p. ISBN 978-3-527-33197-0.

[2] NAGARAJAN, R and T HATTON. *Nanoparticles: synthesis, stabilization, passivation, and functionalization*. New York: Oxford University Press, 2008, xiv, 449 p., 1 leaf of plates. ISBN 978-0-8412-6969-9.

[3] High Tech Art: Chameleon Glass. In: [online]. 1993. pub. S.l.: U S Govt Printing Office, 1993 [cit. 2015-04-26]. ISBN 0160421004. Available from: `http://ntrs.nasa.gov/archive/nasa/casi.ntrs.nasa.gov/20020080952.pdf`.

[4] FREESTONE, Ian, Nigel MEEKS, Margaret SAX and Catherine HIGGITT. The Lycurgus Cup — A Roman nanotechnology. *Gold Bulletin* [online]. 2007, vol. 40, issue 4, p. 270-277 [cit. 2015-04-26]. DOI: 10.1007/BF03215599. Available from: `http://link.springer.com/10.1007/BF03215599`.

[5] DREXLER, Eric. "There's Plenty of Room at the Bottom": (Richard Feynman, Pasadena, 29 December 1959) — Metamodern. In: [online]. 2009. pub. [cit. 2015-04-26]. Available from: `http://metamodern.com/2009/12/29/theres-plenty-of-room-at-the-bottom%E2%80%9D-feynman-1959/`.

[6] *Nanoparticles: From Theory to Application*. 2nd ed., completely rev. and updated ed. Editor Günter Schmid. Weinheim: Wiley-VCH, 2010, xiii, 522 p. ISBN 978-3-527-32589-4.

[7] HOUTEPEN, Arjan and Michiel KREUTZER. Nanoparticles in the liquid phase - synthesis and applications. In: [online]. Delft University of Technology [cit. 2015-04-26]. Available from: `http://www2.msm.ctw.utwente.nl/sluding/TEACHING/ParticleTechnology/Kreutzer_WetNanoparticles.pdf`.

[8] Quantum Dots. In: [online]. [cit. 2015-04-26]. Available from: `http://www.sigmaaldrich.com/materials-science/nanomaterials/quantum-dots.html`.

[9] What's So Special about the Nanoscale. In: [online]. [cit. 2015-04-26]. Available from: `http://www.nano.gov/nanotech-101/special`.

[10] Particle Formation: Theory of Nucleation and Systems. In: [online]. Max Planck Institute of Colloids and Interfaces [cit. 2015-04-26]. Available from: `http://www.mpikg.mpg.de/886735/Nucleationlecture.pdf`.

[11] SEAR, Richard P. Nucleation: theory and applications to protein solutions and colloidal suspensions. *Journal of Physics: Condensed Matter*. 2007-01-24, vol. 19, issue 3, p. 033101-. DOI: 10.1088/0953-8984/19/3/033101. Available from: `http://stacks.iop.org/0953-8984/19/i=3/a=033101?key=crossref.dc58db57e07ad4dd93b0f4ba3408cdec`.

[12] THANH, Nguyen T. K., N. MACLEAN and S. MAHIDDINE. Mechanisms of Nucleation and Growth of Nanoparticles in Solution. *Chemical Reviews*. 2014-08-13, vol. 114, issue 15, p. 7610-7630. DOI: 10.1021/cr400544s. Available from: `http://pubs.acs.org/doi/abs/10.1021/cr400544s`.

[13] PRUPPACHER, Hans R and James D KLETT. *Microphysics of clouds and precipitation*. 2nd rev. and enl. ed. Boston: Kluwer Academic Publishers, 1997, xx, 954 p. ISBN 07-923-4211-9.

[14] SEAR, Richard P. Quantitative studies of crystal nucleation at constant supersaturation: experimental data and models. *CrystEngComm*. 2014, vol. 16, issue 29, p. 6506-6522. DOI: 10.1039/C4CE00344F. Available from: `http://xlink.rsc.org/?DOI=C4CE00344F`.

[15] ABRAHAM, Farid F. *Homogeneous nucleation theory: the pretransition theory of vapor condensation*. New York: Academic Press, 1974, xiv, 263 p. ISBN 01-203-8361-6.

[16] DEMELLO, John and Andrew DEMELLO. Microscale reactors: nanoscale products. *Lab on a Chip*. 2004, vol. 4, issue 2, 11N-15N. DOI: 10.1039/b403638g. Available from: `http://xlink.rsc.org/?DOI=b403638g`.

[17] PICRAUX, Tom. Nanofabrication. In: [online]. [cit. 2015-04-27]. Available from: `http://www.britannica.com/EBchecked/topic/962484/nanotechnology/236451/Communications#toc236452`.

[18] VOLLATH, D. *Nanoparticles - Nanocomposites - Nanomaterials: An Introduction for Beginners*. Weinheim: Wiley-VCH, 2013, ix, 310 p. ISBN 978-352-7334-605.

[19] NI, Yong-hong, Xian-wen WEI, Jian-ming HONG and Yin YE. Hydrothermal preparation and optical properties of ZnO nanorods. *Materials Science and Engineering: B*. 2005, vol. 121, 1-2, p. 42-47. DOI: 10.1016/j.mseb.2005.02.065.

[20] SAHOO, Yudhisthira, Alireza GOODARZI, Mark T. SWIHART, Tymish Y. OHULCHANSKYY, Navjot KAUR, Edward P. FURLANI and Paras N. PRASAD. Aqueous Ferrofluid of Magnetite Nanoparticles: Fluorescence Labeling and Magnetophoretic Control. *The Journal of Physical Chemistry B*. 2005, vol. 109, issue 9, p. 3879-3885. DOI: 10.1021/jp045402y.

[21] ŠIMŠÍKOVÁ, Michaela, Jan ČECHAL, Anna ZORKOVSKÁ, Marián ANTALÍK and Tomáš ŠIKOLA. Preparation of CuO/ZnO nanocomposite and its application as a cysteine/homocysteine colorimetric and fluorescence detector. *Colloids and Surfaces B: Biointerfaces*. 2014, vol. 123, p. 951-958. DOI: 10.1016/j.colsurfb.2014.10.051. Available from: `http://linkinghub.elsevier.com/retrieve/pii/S0927776514006055`.

[22] GUBIN, S. *Magnetic nanoparticles*. Weinheim: Wiley-VCH, 2009, xiv, 466 p. ISBN 35-274-0790-1.

[23] ERNST, W. *Earth materials*. Englewood Cliffs, N.J.: Prentice-Hall, [1969], viii, 149 p. ISBN 978-0132226042.

[24] TURKEVICH, John, Peter Cooper STEVENSON and James HILLIER. A study of the nucleation and growth processes in the synthesis of colloidal gold. *Discussions of the Faraday Society*. 1951, vol. 11. DOI: 10.1039/df9511100055.

[25] BRUST, Mathias, Merryl WALKER, Donald BETHELL, David J. SCHIFFRIN and Robin WHYMAN. Synthesis of thiol-derivatised gold nanoparticles in a two-phase Liquid?Liquid system. *Journal of the Chemical Society, Chemical Communications*. 1994, issue 7, p. 801-. DOI: 10.1039/c39940000801. Available from: `http://xlink.rsc.org/?DOI=c39940000801`.

[26] PERRAULT, Steven D. and Warren C. W. CHAN. Synthesis and Surface Modification of Highly Monodispersed, Spherical Gold Nanoparticles of 50-200 nm. *Journal of the American Chemical Society*. 2009-12-02, vol. 131, issue 47, p. 17042-17043. DOI: 10.1021/ja907069u. Available from: `http://pubs.acs.org/doi/abs/10.1021/ja907069u`.

[27] MARTIN, Matthew N., James I. BASHAM, Paul CHANDO and Sang-Kee EAH. Charged Gold Nanoparticles in Non-Polar Solvents: 10-min Synthesis and 2D Self-Assembly. *Langmuir*. 2010-05-18, vol. 26, issue 10, p. 7410-7417. DOI: 10.1021/la100591h. Available from: `http://pubs.acs.org/doi/abs/10.1021/la100591h`.

[28] LI, Chunfang, Dongxiang LI, Gangqiang WAN, Jie XU and Wanguo HOU. Facile synthesis of concentrated gold nanoparticles with low size-distribution in water: temperature and pH controls. *Nanoscale Research Letters*. 2011, vol. 6, issue 1. DOI: 10.1186/1556-276x-6-440.

[29] Gold nanoparticles. In: [online]. [cit. 2015-04-27]. Available from: http://www.chimica.unipd.it/fabrizio.mancin/pubblica/Nanobiotech/VII%20lezione.pdf.

[30] Synthesis of aqueous Gold Nanoparticles. In: [online]. [cit. 2015-04-27]. Available from: http://chem553project.wikispaces.com/Synthesis+of+aqueous+Gold+Nanoparticles.

[31] ZHOU, Jingfang, John RALSTON, Rossen SEDEV and David A. BEATTIE. Functionalized gold nanoparticles: Synthesis, structure and colloid stability. *Journal of Colloid and Interface Science*. 2009, vol. 331, issue 2, p. 251-262. DOI: 10.1016/j.jcis.2008.12.002. Available from: http://linkinghub.elsevier.com/retrieve/pii/S0021979708016019.

[32] PERALA, Siva Rama Krishna and Sanjeev KUMAR. On the Mechanism of Metal Nanoparticle Synthesis in the Brust–Schiffrin Method. *Langmuir*. 2013-08-06, vol. 29, issue 31, p. 9863-9873. DOI: 10.1021/la401604q. Available from: http://pubs.acs.org/doi/abs/10.1021/la401604q.

[33] GUPTA, Ram B and Uday B KOMPELLA. *Nanoparticle technology for drug delivery*. New York: Taylor, 2006, xiii, 403 p. ISBN 15-744-4857-9.

[34] Tyndall effect. In: [online]. [cit. 2015-04-27]. Available from: http://www.britannica.com/EBchecked/topic/611583/Tyndall-effect.

[35] MCMULLAN, D. SCANNING ELECTRON MICROSCOPY 1928 - 1965. In: [online]. Cavendish Laboratory, University of Cambridge, UK, 1993 [cit. 2015-04-28]. Available from: http://www-g.eng.cam.ac.uk/125/achievements/mcmullan/mcm.htm.

[36] EDITED BY PAUL L.H. MCSWEENEY, Edited by Paul L.H.Patrick F. *Advanced dairy chemistry. basic aspects*. 4th ed. New York: Springer, 2013. ISBN 978-146-1447-139.

[37] The Tyndall Effect. In: [online]. [cit. 2015-04-28]. Available from: http://www.science20.com/square_root_of_not/the_tyndall_effect-153383.

[38] ABRAMOWITZ, Mortimer and Michael W. DAVIDSON. Anatomy of the Microscope: Introduction. In: [online]. [cit. 2015-04-28]. Available from: http://www.olympusmicro.com/primer/anatomy/introduction.html.

[39] BORN, Max. *Principles of Optics. Electromagnetic Theory of Propagation, Interference and Diffraction of Light*. 6 ed. Cambridge: University Press, 1997, 808 s. ISBN 05-216-3921-2.

[40] The Nobel Prize in Chemistry 2014. In: *Nobelprize.org* [online]. Nobel Media AB 2014 [cit. 2015-04-28]. Available from: http://www.nobelprize.org/nobel_prizes/chemistry/laureates/2014/.

[41] VON ARDENNE, Manfred. Das Elektronen-Rastermikroskop. *Zeitschrift für Physik*. 1938, vol. 109, 9-10, p. 553-572. DOI: 10.1007/BF01341584. Available from: http://link.springer.com/10.1007/BF01341584.

[42] KOLÍBALOVÁ, Eva. Introduction to Scanning Electron Microscopy. In: [online]. [cit. 2015-04-28]. Available from: http://physics.fme.vutbr.cz/files/116/Specialni%20praktika%20I%20Dvorak/SEM_2.pdf.

[43] Microscopy. In: [online]. [cit. 2015-04-28]. Available from: http://www.ualberta.ca/~ccwj/teaching/microscopy/.

[44] CLARK, Jim. THE BEER-LAMBERT LAW. In: [online]. [cit. 2015-05-21]. Available from: http://www.chemguide.co.uk/analysis/uvvisible/beerlambert.html.

[45] Photoluminescence (PL). In: [online]. [cit. 2015-05-21]. Available from: http://www.horiba.com/scientific/products/photoluminescence/.

[46] Photoluminescence explained. In: [online]. [cit. 2015-05-21]. Available from: http://www.renishaw.com/en/photoluminescence-explained--25809.

[47] PREUS, Søren. Fluorescence Quantum Yield. In: [online]. [cit. 2015-05-26]. Available from: http://www.fluortools.com/software/ae/documentation/qy.

[48] SCHASFOORT, R and Anna J TUDOS. *Handbook of surface plasmon resonance*. Cambridge, UK: RSC Pub., 2008, xxi, 403 p. ISBN 08-540-4267-9.

[49] Surface Plasmon Resonance. In: [online]. [cit. 2015-04-28]. Available from: http://www.unitus.it/biophysics/RicercaEn_file/spr%20sito.htm.

[50] COOPER, Matthew A. Optical biosensors in drug discovery. *Nature Reviews Drug Discovery*. July 2002, vol. 1, issue 7, p. 515-528. DOI: 10.1038/nrd838. Available from: http://www.nature.com/doifinder/10.1038/nrd838.

[51] Gold Nanoparticles: Properties and Applications. In: [online]. [cit. 2015-04-28]. Available from: http://www.sigmaaldrich.com/materials-science/nanomaterials/gold-nanoparticles.html.

[52] MODY, VickyV, Rodney SIWALE, Ajay SINGH and HardikR MODY. Introduction to metallic nanoparticles. *Journal of Pharmacy and Bioallied Sciences*. 2010, vol. 2, issue 4, p. 282-. DOI: 10.4103/0975-7406.72127. Available from: http://www.jpbsonline.org/text.asp?2010/2/4/282/72127.

[53] FRIEDMAN, Lawrence M, Curt FURBERG and David L DEMETS. *Fundamentals of clinical trials*. 4th ed. New York: Springer, 2010, xviii, 445 p. ISBN 978-144-1915-863.

[54] GHOSH, P, G HAN, M DE, C KIM and V ROTELLO. Gold nanoparticles in delivery applications. *Advanced Drug Delivery Reviews*. 2008-08-17, vol. 60, issue 11, p. 1307-1315. DOI: 10.1016/j.addr.2008.03.016. Available from: http://linkinghub.elsevier.com/retrieve/pii/S0169409X08000999.

[55] CONDE, João, Gonçalo DORIA and Pedro BAPTISTA. Noble Metal Nanoparticles Applications in Cancer. *Journal of Drug Delivery*. 2012, vol. 2012, p. 1-12. DOI: 10.1155/2012/751075. Available from: http://www.hindawi.com/journals/jdd/2012/751075/.

[56] PRABHU, Sukumaran and Eldho K POULOSE. Silver nanoparticles: mechanism of antimicrobial action, synthesis, medical applications, and toxicity effects. *International Nano Letters*. 2012, vol. 2, issue 1, p. 32-. DOI: 10.1186/2228-5326-2-32. Available from: http://www.inl-journal.com/content/2/1/32.

[57] PEARSON, Ralph G. Hard and Soft Acids and Bases. *Journal of the American Chemical Society*. 1963, vol. 85, issue 22, p. 3533-3539. DOI: 10.1021/ja00905a001. Available from: http://pubs.acs.org/doi/abs/10.1021/ja00905a001.

[58] LEE, Hyang Yeon, Hyoung Kun PARK, Yoon Mi LEE, Kwan KIM and Seung Bum PARK. A practical procedure for producing silver nanocoated fabric and its antibacterial evaluation for biomedical applications. *Chemical Communications*. 2007, issue 28, p. 2959-. DOI: 10.1039/b703034g. Available from: http://xlink.rsc.org/?DOI=b703034g.

[59] KLINGSHIRN, C. ZnO: Material, Physics and Applications. *ChemPhysChem*. 2007-04-23, vol. 8, issue 6, p. 782-803. DOI: 10.1002/cphc.200700002. Available from: http://doi.wiley.com/10.1002/cphc.200700002.

[60] Zinc Oxide Applications. In: [online]. [cit. 2015-05-21]. Available from: http://www.zinc.org/info/zinc_oxide_applications.

[61] CHANG, Tongqin, Zijiong LI, Gaoqian YUN, Yong JIA and Hongjun YANG. Enhanced Photocatalytic Activity of ZnO/CuO Nanocomposites Synthesized by Hydrothermal Method. *Nano-Micro Letters*. 2013, vol. 5, issue 3, p. 163-168. DOI: 10.1007/BF03353746. Available from: http://link.springer.com/10.1007/BF03353746.

[62] KETCHIE, W, Y FANG, M WONG, M MURAYAMA and R DAVIS. Influence of gold particle size on the aqueous-phase oxidation of carbon monoxide and glycerol. *Journal of Catalysis*. 2007-08-15, vol. 250, issue 1, p. 94-101. DOI: 10.1016/j.jcat.2007.06.001. Available from: http://linkinghub.elsevier.com/retrieve/pii/S0021951707002205.

[63] SAU, Tapan K. and Catherine J. MURPHY. Seeded High Yield Synthesis of Short Au Nanorods in Aqueous Solution. *Langmuir*. 2004, vol. 20, issue 15, p. 6414-6420. DOI: 10.1021/la049463z. Available from: http://pubs.acs.org/doi/abs/10.1021/la049463z.

[64] SONAVANE, Ganeshchandra, Keishiro TOMODA and Kimiko MAKINO. Biodistribution of colloidal gold nanoparticles after intravenous administration: Effect of particle size. *Colloids and Surfaces B: Biointerfaces*. 2008, vol. 66, issue 2, p. 274-280. DOI: 10.1016/j.colsurfb.2008.07.004. Available from: http://linkinghub.elsevier.com/retrieve/pii/S0927776508002695.

LIST OF ABBREVIATIONS

Abbreviation	Meaning
CVD	Chemical Vapour Deposition
PVD	Physical Vapour Deposition
QD	Quantum Dot
AO	Atomic Orbital
MOs	Molecular Orbitals
AuNP	Gold Nanoparticle
AgNP	Silver Nanoparticle
SEM	Scanning Electron Microscopy
TEM	Transmission Electron Microscopy
AFM	Atomic Force Microscopy
PL	Photoluminiscence
QY	Quantum Yield
SPR	Surface Plasmon Resonance
SERS	Surface-enhanced Raman Spectroscopy
DNA	Deoxyribonucleic Acid
RNA	Ribonucleic Acid
MRI	Magnetic Resonance Imaging
CT	Computed Tomography
PET	Positron Emission Tomography
UV	Ultraviolet
MB	Methylene Blue
MO	Methylene Orange
Cys	Cystein
Hcy	Homocystein
DW	Deionized Water
TC	Trisodium Citrate Dihydrate
CPS	Counts Per Second
SE	Secondary Electrons
STEM	Scanning Transmission Electron Microscopy